Research article

JGS
Journal of the Geological Society

Published Online First

https://doi.org/10.1144/jgs2020-226

A revised age, structural model and origin for the North Pennine Orefield in the Alston Block, northern England: intrusion (Whin Sill)-related base metal (Cu–Pb–Zn–F) mineralization

E. D. Dempsey[1], R. E. Holdsworth[2,3], D. Selby[2,4], A. Bird[1], B. Young[2] and C. Le Cornu[2,5]

[1] Department of Geography, Geology and Environment, University of Hull, Hull HU6 7RX, UK
[2] Department of Earth Sciences, Durham University, Durham DH1 3LE, UK
[3] Geospatial Research Ltd, Harrison House, Durham DH1 4EL, UK
[4] State Key Laboratory of Geological Processes and Mineral Resources, School of Earth Resources, China University of Geosciences, Wuhan, 430074, Hubei, China
[5] Centamin, 2 Mulcaster Street, St Helier, Jersey, JE2 3NJ, UK

REH, 0000-0002-3467-835X
Correspondence: r.e.holdsworth@durham.ac.uk

Abstract: Mineralization and associated fluid migration events in the *c.* 1500 km^2 North Pennine Orefield (NPO) are known to be associated with tectonic activity, but the age of these tectonic events and origins of the base metal sulfide mineralization remain unresolved. New fieldwork in the Alston Block shows that mineralization post-dates a weakly developed phase of north–south shortening consistent with far-field Variscan basin inversion during the late Carboniferous. New observations of field relationships, coupled with microstructural observations and stress inversion analyses, together with Re–Os sulfide geochronology show that the vein-hosted mineralization (apart from barium minerals) was synchronous with a phase of north–south extension and east–west shortening coeval with emplacement of the Whin Sill (*c.* 297–294 Ma). Thus the development of the NPO was related to an early Permian regional phase of transtensional deformation, mantle-sourced hydrothermal mineralization and magmatism in northern Britain. Previously proposed Mississippi Valley Type models, or alternatives relating mineralization to the influx of Mesozoic brines, can no longer be applied to the development of the NPO in the Alston Block. Our findings also mean that existing models for equivalent base metal sulfide fields worldwide (e.g. Zn–Pb districts of Silesia, Poland and Tennessee, USA) may need to be reassessed.

Received 23 November 2020; **revised** 21 January 2021; **accepted** 26 January 2021

The world-famous veins and orebodies of the North Pennine Orefield (NPO) have long been considered to be archetypal examples of a Mississippi Valley Type (MVT) deposit (e.g. Halliday *et al.* 1990, and references therein) and have been exploited since at least the 12th century. The NPO covers an area of *c.* 1500 km^2 and by the time mining activities ceased during the early 20th century, *c.* 10×10^6 tonnes of ore (Zn, Pb, Ba, Fe, Cu) had been extracted (Dunham 1944, 1990). The orefield lies at the centre of a structural high known as the Alston Block, a *c.* 40 km wide, fault-bounded horst (Fig. 1a). The block is bounded to the north by the Stublick–Ninety Fathom Fault system, to the south by the Lunedale–Butterknowle Fault system, and to the west by the Pennine Fault system. Although it is generally agreed that mineralization was contemporaneous with tectonic activity in conjunction with fluid migration, the age of these tectonic events and origin of sulfide mineralization remain unresolved. Here we integrate detailed field observations, palaeostress analyses of fault slickenline data and rhenium–osmium (Re–Os) geochronology and geochemistry on vein-hosted pyrite samples to constrain the style and timing of events relating to the genesis of the NPO and the structural evolution of the Alston Block and adjacent regions of northern England.

Geological setting

The Alston Block and the North Pennine batholith

The geological structure of northern England is dominated by features associated with basin formation during the Carboniferous. North–south Early Mississippian (*c.* 359–335 Ma) rifting is widely recognized (Underhill *et al.* 1988; Collier 1989) and is characterized by the formation of a series of fault-bounded basins and structural highs. Of these, the Alston Block separates the Northumberland Trough to the north from the Stainmore Trough to the south and is bounded to the west by the post-Carboniferous Pennine escarpment and Vale of Eden basin (Fig. 1a). The Alston Block preserves a 600 m thick sedimentary sequence of Carboniferous cyclothemic sedimentary rocks, which range in age from the Late Mississippian to Pennsylvanian (*c.* 335–300 Ma age). They lie unconformably upon a basement block of deformed Paleozoic sedimentary and volcanic rocks intruded by the North Pennine batholith (Dunham 1990; *c.* 399 Ma, Re–Os molybdenite, U–Pb chemical abrasion isotope dilution thermal ionization mass spectrometry (CA-ID-TIMS) zircon; Selby *et al.* 2008; Kimbell *et al.* 2010) (Fig. 1a and b). The erosional non-conformity that separates the North Pennine batholith and the Carboniferous strata (Dunham *et al.* 1961) rules out any direct genetic link between the NPO mineralization and batholith emplacement. The presence of this low-density granitic core ensured that the Alston Block was underlain by relatively buoyant crust during Early Mississippian rifting, forming a prominent fault-bounded structural high (Critchley 1984). This resulted in a Carboniferous cover sequence across the block that is relatively thin compared with those within the surrounding basins (Collier 1989; Chadwick *et al.* 1995). Rifting was superseded by thermal subsidence during the Late Carboniferous (Bott *et al.* 1984).

The effects of Late Carboniferous shortening and inversion are well documented throughout the basins surrounding the Alston Block (e.g. Shiells 1963) and have been attributed by some

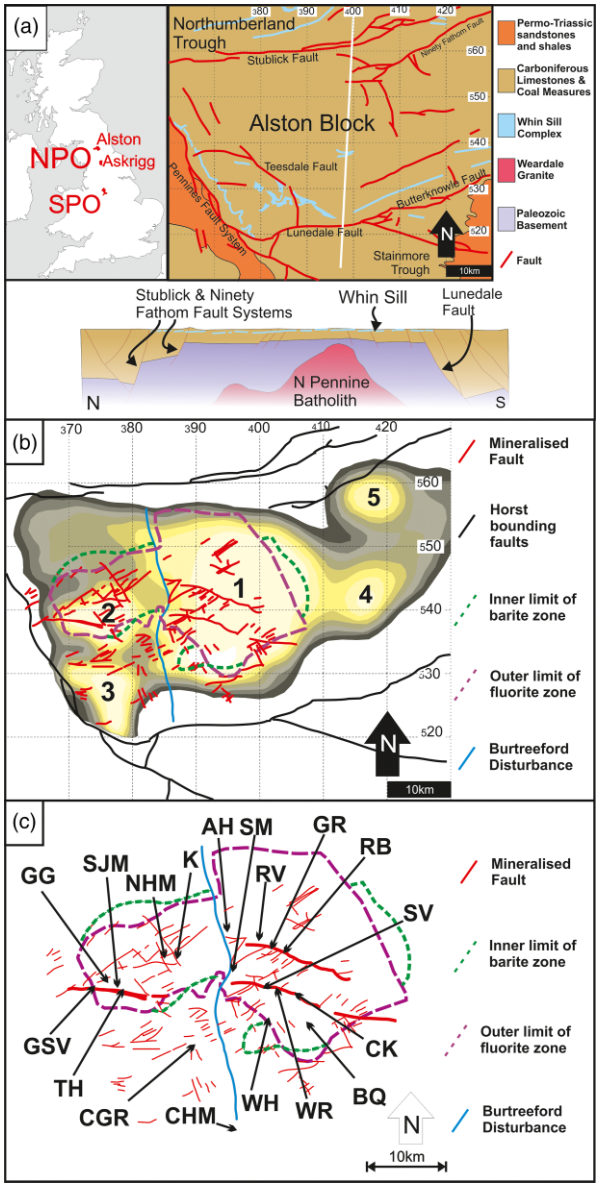

Fig. 1. (**a**) Simplified geological map and schematic north–south cross-section of the Alston Block based on the line of section (white). (**b**) The main mineralized faults (red) of the main NPO plotted over the five plutons of the Weardale granite (1, Weardale Pluton; 2, Tynehead Pluton; 3, Scordale Pluton; 4, Cornsay Pluton; 5, Rowlands Gill Pluton). The depth contours to the top of the granite are also shown in dark grey (deepest) to white (shallowest) (based on Kimbell *et al.* 2010). (**c**) Locations of localities and features mentioned in the text: GG, Garrigill; SJM, Sir John's Mine; NHM, Nenthead; K, Killhope; SM, Sedling Mine; AH, Allenheads; RV, Red Vein; GR, Groverake Mine; RB, Redburn; CK, Cambokeels, BQ, Bollihope Quarry; WR, West Rigg workings; WH, Westernhope; SV, Slitt Vein; CHM, Closehouse Mine; CGR, Cow Green Reservoir; TH, Tynehead; GSV, Great Sulphur Vein.

researchers to the far-field effects of the Variscan Orogeny (e.g. Corfield *et al.* 1996). However, evidence for north–south shortening within the Alston Block has proved to be elusive, leading to suggestions that the underlying North Pennine batholith acted as a shield, protecting the overlying Carboniferous cover sequence from regional compressive stresses (e.g. Critchley 1984). The most obvious evidence of Late Carboniferous inversion is preserved along the southern edge of the Alston Block where the Lunedale Fault (Fig. 1a) has been reactivated as a top-to-the north reverse fault (Cornwell and Wadge 1980; Dunham 1990). Large-scale gentle east–west elongated doming of the Carboniferous sediments, known as the Teesdale Dome (Dunham 1931), has also been interpreted to have formed during the Late Carboniferous owing to Variscan shortening (Dunham 1990).

Early Permian magmatism and the Burtreeford Disturbance.

The Late Carboniferous to Early Permian was a time of widespread magmatism across NW Europe (e.g. Timmerman 2004). The main manifestation in northern England is the doleritic Whin Sill Complex (Fig.1a; Francis 1982), dated at 297.4 ± 0.4 Ma (U–Pb baddeleyite; Hamilton and Pearson 2011), which formed during a period of large-scale lithospheric extension. In northern England, the ENE–WSW-trending Holy Island and High Green dykes (Whin Sill feeder dykes) show en-echelon geometries consistent with emplacement during east–west shortening synchronous with broadly north–south extension. This correlates well with the dextral transtensional deformation documented in the Northumberland Basin during the Late Carboniferous–Early Permian, which is considered to be contemporaneous with intrusion of the Whin Sill based on cross-cutting relationships with associated mineral veins (De Paola *et al.* 2005*a*).

The Burtreeford Disturbance (Fig. 1b) is a major structural feature of the Alston Block, although, because it is rarely exposed at the surface and has been penetrated by only a very small number of mine workings, it is poorly understood in detail (Dunham 1990). It is a north–south-trending, east-facing monocline, which lies between the Tynehead and Scordale plutons and the larger Weardale pluton of the North Pennine batholith (Fig. 1b). It has an eastward downthrow of up to 150 m and has been interpreted as being active both during and after emplacement of the Whin Sill (Hill and Dunham 1968; Astle 1978; Johnson and Dunham 2001). The Burtreeford Disturbance is proposed to represent a northern continuation of the Dent Line, which is thought to be the surface manifestation of a much deeper ancient Devonian north–south wrench fault zone (Underhill *et al.* 1988; Woodcock and Rickards 2003). Similar structures exposed in the Lake District (Moseley 1972) are thought to be related to regional sinistral shear during the Acadian Orogeny. During Late Carboniferous–Early Permian inversion, the Dent Line underwent sinistral transpressional reactivation, forming a large monoclinal structure before finally undergoing sinistral transtension during the Early Permian (Underhill *et al.* 1988; Thomas and Woodcock 2015).

Mineralization of the North Pennine Orefield

The majority of mineralization within the NPO is hosted by the Carboniferous strata. Little is known of any mineralization characteristic of the NPO within the underlying Lower Paleozoic basement rocks, although narrow veins of fluorite, quartz and sulfides are observed in the Rookhope Borehole from the granite of the batholith's Weardale pluton (Dunham *et al.* 1965). Within the Carboniferous, the NPO deposits are hosted within and related to, if not controlled by, regional faults and fractures in four main orientations: NNW–SSE ('Cross Veins'), NE–SW ('Lead Veins'), ENE–WSW and WNW–ESE ('Quarter Point veins'), with the NNW–SSE set notably lacking significant mineralization (Fig. 1a) (Dunham 1990). In addition to vein-fillings, the mineralization includes numerous strata-bound Pb–Zn–Fe replacement deposits, or 'flats', developed in limestone wall rocks in close proximity to mineralized faults. The deposits of the NPO are characterized by an abundance of sulfide ores, dominated by galena and sphalerite, although with local smaller concentrations of chalcopyrite, pyrite, pyrrhotite, marcasite and rare traces of bismuth, cobalt and nickel sulfides. The main gangue minerals are fluorite, quartz (of various forms), barium minerals, abundant siderite and ankerites of various

compositions. Calcite, together with small amounts of aragonite, is widespread, although almost invariably in only minor amounts.

Although it is generally agreed that mineralization was contemporaneous with tectonic activity in conjunction with fluid migration, the age of these tectonic events and origin of sulfide mineralization in the NPO has remained enigmatic. A number of different techniques used to date this mineralization have yielded wide-ranging dates that vary between 290 and 149 Ma (e.g. Dunham *et al.* 1968; Solomon *et al.* 1971; Shepherd *et al.* 1982; Dunham 1990; Halliday *et al.* 1990; Davison *et al.* 1992). As several of the orefield's vein deposits are hosted in fractures that cross-cut parts of the Whin Sill complex, this has commonly been used to infer that mineralization postdates Whin Sill magmatism (e.g. Dunham 1934, 1990; Cann and Banks 2001). Given that large-scale faults, such as the 90-Fathom Fault System, are also known to offset both the Whin Sill complex and Permian strata (Collier 1989; De Paola *et al.* 2005*b*), this could suggest that fault reactivation, and perhaps mineralization, occurred during, or was continuous into the Mesozoic (Cann and Banks 2001).

Perhaps the most conspicuous feature of NPO mineralization is the marked zonal distribution of major constituent minerals, most notably fluorite and barium minerals. Fluorite mineralization occurs within an inner zone, centred above the three westernmost plutons of the North Pennine batholith (Weardale, Tynehead and Scordale); insufficient data exist to infer any relationships with the eastern (Rowlands Gill and Cornsay) plutons, although barium mineralization is abundantly present in several fracture systems above the latter. Barium mineralization occurs almost exclusively outside the fluorite zone (Fig. 1b) and it was this zonal pattern that guided much of the early thinking on the origins and evolution of the field and on the possible presence of a concealed granitic body (Dunham 1934).

Several genetic models have since been put forward for the age and formation of the NPO. Dunham (1983) advocated classifying the NPO as a fluoritic sub-type of the MVT, a concept developed further by Halliday *et al.* (1990), who suggested that metals were leached from the Carboniferous host rocks at *c.* 200 Ma (Early Jurassic) by circulating proximal connate fluids. This was based on a range of εNd values consistent with a Carboniferous source mineralizing at 200 Ma, with this age being derived from Rb/Sr isotopic data obtained from fluid inclusions in the Great Sulphur Vein (Fig. 1a; Shepherd *et al.* 1982). An unusual assemblage of magnetite, silicate minerals and ore minerals including niccolite, galena and sphalerite, associated with the NNW–SSE-trending Teesdale Fault, was interpreted by Young *et al.* (1985) as a skarn assemblage resulting from the interaction of metal-rich mineralizing fluids with the Whin Sill and its contact rocks very soon after the sill's emplacement and whilst still at temperatures in excess of 500°C. Crowley *et al.* (1997) presented isotopic evidence for the derivation of at least some of the sulfur in barite from both the NPO and northern Lake District from deeply buried Carboniferous evaporites in the Solway–Northumberland Basin.

More recently, Cann and Banks (2001) proposed an alternative model in which initial deep fluid movement in the granitic basement below the Alston Block was prevented during the Carboniferous by sealing of pre-existing cracks allowing temperatures to rise to 200°C, up to 100°C hotter than the surrounding country rocks. They hypothesized that Late Permian tectonic extension allowed saline waters from the Zechstein Sea to penetrate deep into the basement where they became heated to as much as 200°C. This led to a 'chimney effect', which generated concentric zones of increasing temperature fluid and mineralization in the Carboniferous host rocks centred over the batholith buried at depth. Earlier workers, notably Johnson and Dunham (1963), had also proposed a series of 'emanative centres' of mineralization, most notably at a triple junction of veins at Groverake Mine in Rookhope where temperatures derived from subsequent fluid inclusion results, together with rare earth element (REE) studies, gave strong support to this model (Ixer *et al.* 1996). In describing the Great Sulphur Vein of Alston Moor, Dunham (1990) noted that quartz-dominated mineralization gives way at depth to a zone rich in iron and minor copper sulfides and suggested that this reflected a thermal gradient in the upwelling fluids. Very similar changes to vein contents, with a marked increase in iron sulfide mineralization, have subsequently been observed at depth in recent fluorspar workings on the Quarter Point Slitt Vein at Cambokeels Mine in Weardale and similar features were observed in the deepest workings in the Quarter Point Red Vein system at Groverake Mine in Rookhope. More recently, Bouch *et al.* (2006) have pointed out that the inner boundary of the cooler barium zone does not coincide precisely with the outer boundary of the hotter fluorite zone and that they may represent two distinct and unrelated mineralization events. This suggestion is consistent with the observation that across the NPO the occurrences of fluorite and barium minerals are almost always mutually exclusive. Bott and Smith (2018) have shown, based on thermal conductivity and geophysical modelling, that the North Pennine batholith was unlikely to have been hot enough to generate the chimney effect proposed. Instead, they suggested that alkali magma underplating the batholith, associated with the intrusion of the Whin Sill Complex during the earliest Permian, is the only viable way to account for the observed mineralization.

Many of the uncertainties about the age and genesis of the NPO centre around the issue of the relative and absolute timings of faulting, mineralization and igneous intrusion in the Alston Block. In this paper, we combine detailed field, microstructural and geochemical analyses to address the timing and affinities of the mineralization and assess its relationship to regional magmatism of the Whin Sill Complex in northern England. The present study focuses mainly on relationships observed in the inner fluorite zone where barium minerals are absent. The genesis and structural setting of barium minerals, which are generally late in mineralization sequences outside the fluorite zone in the Alston Block, are not discussed in detail here.

Field and laboratory methods

Fieldwork

Fieldwork concentrated on key representative localities in a number of abandoned quarries, stream sections and mine workings identified from previous studies. This work focused on the collection of orientation and kinematic data (faults and fractures, mineralized lineations and slickenlines, shear-sense criteria) and oriented samples of mineralized vein fills and fault rocks for thin section and geochemical analysis. All stereonets shown in this paper are equal-area lower-hemisphere plots.

Stress inversion analysis

Fault-slip slickenline data associated with each of the mineralized fault groups identified in the field were used to carry out a conventional palaeostress inversion analysis (Angelier 1979, 1984; Michael 1984) implemented using MyFault® software following the protocols set out by Holdsworth *et al.* (2015) and Dichiarante *et al.* (2020). Importantly, any analysis of this kind is viable only in regions where finite strains are modest and the presence of major fault block rotations can be ruled out. Owing to the small (<2 m) displacements observed along most of the mineralized structures studied, we are confident that regional strain intensities are not large enough to be problematic, and that the degree of rotational strain is negligible (e.g. De Paola *et al.* 2005*a*,*b*; Dempsey *et al.* 2014). The use of 3D Mohr circles derived from the data additionally allows an analysis of the geometric relationships between faults and fractures

measured in the field relative to the orientation and magnitude of the principal stress axes. This can be used to determine which fault and fracture orientations are most susceptible to failure under given stress and pore-fluid pressure conditions (Alaniz-Alvarez *et al.* 1998).

Rhenium–osmium geochronology

Traditionally the relative ages of different deformation events are established using cross-cutting relationships seen in the field and thin section. Although this emphasizes the deformation sequence and gives a relative age, the absolute ages of these events remain unknown in the absence of radiometric dating. Pyrite is commonly enriched with rhenium (Re) so that the ^{187}Re–^{187}Os geochronometer can be used to date mineralization and better constrain the timing of brittle deformation (e.g. Holdsworth *et al.* 2015, 2020; Dichiarante *et al.* 2016). Furthermore, the determined $^{187}Os/^{188}Os$ composition of the sulfide minerals at the time of formation can yield insights into the origins of the fracture-hosted fluids (e.g. Hnatyshin *et al.* 2015).

For this study, pyrite samples, together with one Whin Sill whole-rock sample, were collected *in situ* from spatially diverse veins within the Alston Block NPO (locations shown in Fig. 1b). Pyrite samples were crushed to 2 mm grain size with no metal contact and hand-picked before a final crushing to 75–200 µm. Measurement of the abundance of ^{187}Re and ^{187}Os in pyrite samples is obtained by isotope dilution using a mixed ^{185}Re + ^{190}Os tracer solution, which was calibrated against gravimetric standard solutions of normal isotopic composition. Approximately 400 mg of pyrite or 2 g of Whin Sill (previously dissolved in HF and subsequently dried down to facilitate analysis of silica-bound Re and Os) plus tracer solution was digested in a Carius tube with 8 ml of inverse *aqua regia at 220°C for 48 h.* Rhenium and osmium were separated and purified by solvent extraction ($CHCl_3$) and micro-distillation (Os) and anion exchange chromatography (Re), and analysed by negative thermal ionization mass spectrometry (NTIMS; Selby *et al.* 2009). Uncertainties for Re–Os isotopic data and abundances were determined by full error propagation of uncertainties in mass spectrometer measurements, blank abundances and isotopic compositions, spike calibrations, reproducibility of standard Re and Os mass spectrometric values, and weighing uncertainties. Total procedural blanks were monitored during the three batches of samples run for this study. The average blank measurements over the three batches for Re and Os were 1.7 ± 0.08 ppt and 0.06 ± 0.03 ppt, respectively, with an average $^{187}Os/^{188}Os$ value of 0.28 ± 0.03 (1σ, $n = 3$).

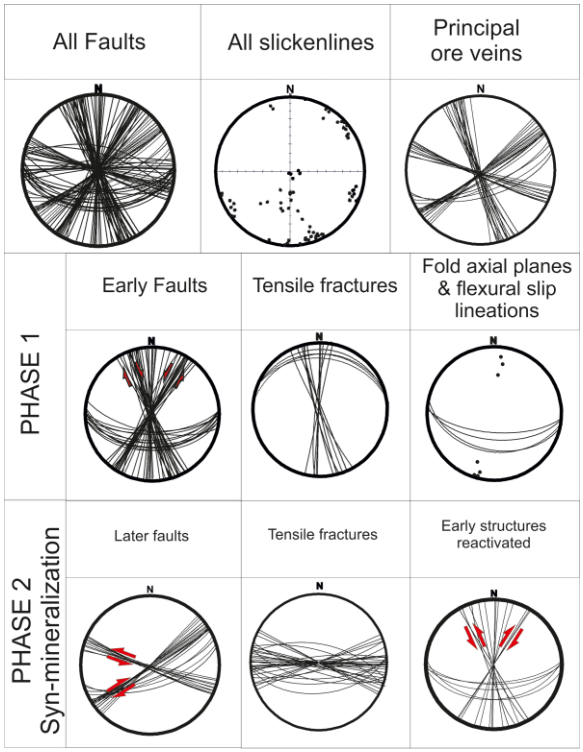

Fig. 2. Stereoplots of fault, vein and fracture sets measured during this study, including slickenline lineations and principal ore veins. Senses of shear where known are also shown for shear fractures attributed to Phases 1 and 2.

Structure of the North Pennine Orefield

The main faults, slickenline and ore vein orientations recorded during the present study are shown in Figure 2. As in previous studies, four main regionally pervasive fault orientations are observed: NE–SW (normal, tensile and dextral) (the 'Lead Veins' of the miners), ESE–WNW 'Quarter Point' (normal, tensile and sinistral), ENE–WSW 'Quarter Point' (dextral) and NNW–SSE 'Cross Veins' (tensile and dextral, locally sinistral). Field observations of cross-cutting relationships documented below show that within the NPO of the Alston Block there are at least two phases of fault initiation, here termed Phase 1 and 2. The Phase 1 NNW–SSE and NNE–SSW fractures, many of which host vein minerals, are predominantly dextral and sinistral strike-slip structures, respectively, and are associated with contemporaneous north–south tensile fractures (Fig. 2). These fractures and veins are commonly cross-cut by Phase 2 mineralized structures (Fig. 2), especially the ESE–WNW veins. There is localized evidence for a later sinistral and dextral reactivation of the NNW–SSE and NNE–SSW structures, respectively, during Phase 2. With a few local exceptions (e.g. Nenthead, South Tyne Valley), the Phase 1 structures are much less mineralized compared with Phase 2. The bulk of mineralization occurs along Phase 2 ESE–WNW (Quarter Point) and NE–SW (Lead Vein) structures, which represent the largest and most continuous features within the Alston Block. Key surface localities analysed during this study are described below. Although there are many exposures of mineralized veins within the Alston Block, the locations described here were selected based on the variety of structures exposed, how representative they are of the regional deformation history and/or their suitability for stress inversion analysis (i.e. slickenlines well preserved). A map showing the locations, structures and veins in the NPO is given in Figure 1c.

Conjugate faults and cross-cutting relationships

Bollihope Quarry [NY9853235254] (Fig. 3a) displays an exceptionally well-exposed 20 m thick sequence of flat-lying Carboniferous Great Limestone gently folded by several large (80 m wavelength) gentle to open folds with shallowly southward plunging (02/175) hinge lines (Fig. 3b). The folds are cross-cut by mineralized brittle shear fractures, but a definitive relative age relationship is not clear (Fig. 3a). Fracture-hosted mineralization within the quarry is dominated by calcite and fluorite, with minor amounts of quartz, pyrite, goethite and galena (Fig. 3c–f). There are four main fracture sets: ENE–WSW dextral, ESE–WNW sinistral, NNW–SSE dextral and NNE–SSW sinistral (Fig. 3a); where preserved, associated slickenlines are shallowly plunging to subhorizontal (Fig. 3e). Field observations show that the ENE–WSW and WNW–ESE sets are conjugate and consistently cross-cut and offset the NNW–SSE and NNE–SSW sets, which are also conjugate. These are interpreted to represent Phase 2 and Phase 1 structures, respectively. The conjugate relationships for each set are identified based on opposing senses of shear and mutually cross-

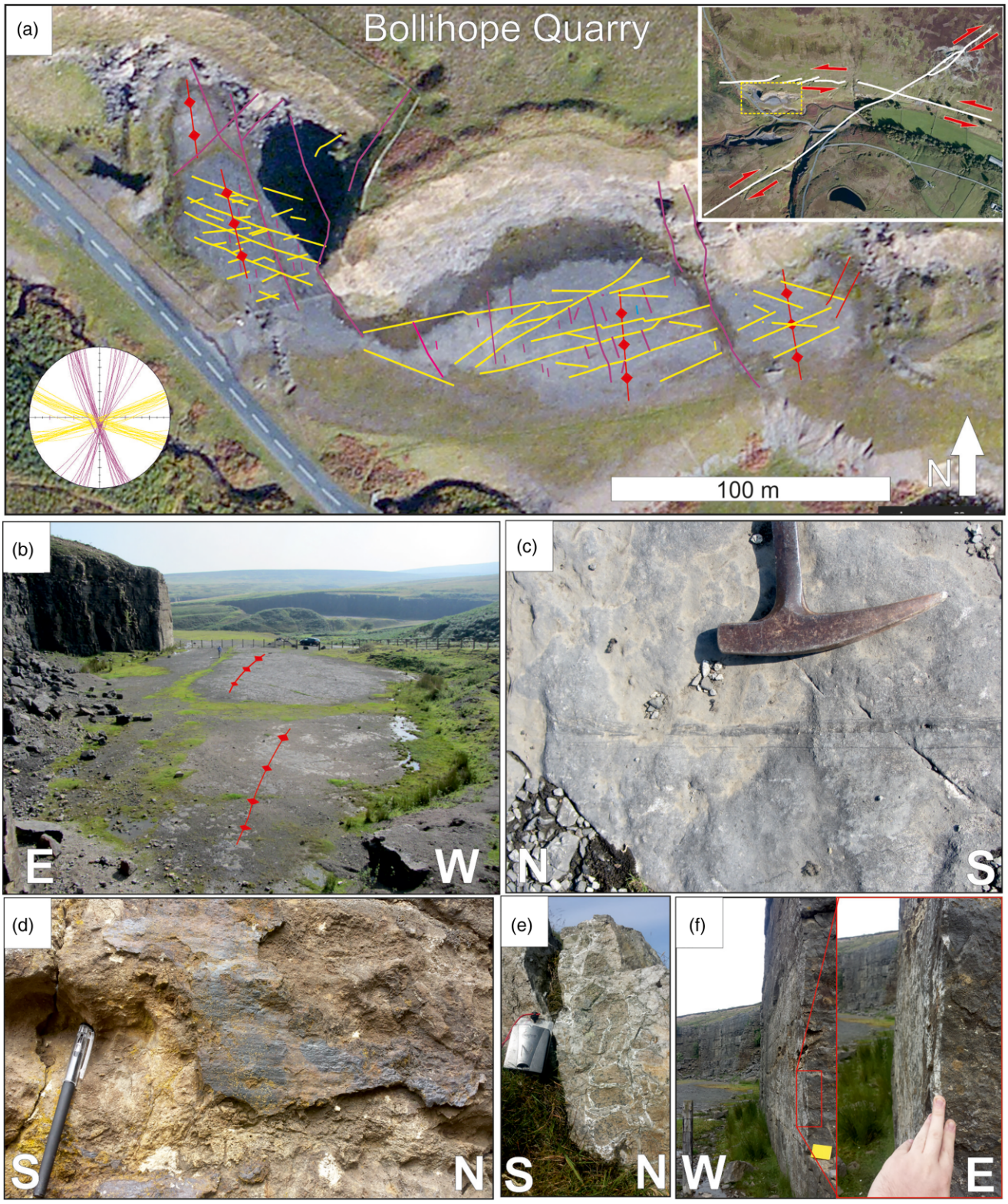

Fig. 3. (**a**) Aerial view of Bollihope Quarry (©Getmapping 23 August 2015 using EDINA Aerial Digimap Service). Mineralized faults traced in yellow, fold hinges in red and tensile veins in purple. The quarry sits adjacent to the intersection of a large ESE–WNW mineralized fault with a large NE–SW fault (inset; yellow box shows location of image in (**a**). (**b**) Oblique view looking south of gentle folding of bedding surface in the limestones forming floor of the quarry. (**c**) Plan view of bedding plane in limestone cut by tensile north–south vein filled with calcite, which has been weathered black. (**d**) Subhorizontal slickenlines with hematite mineralization on NE–SW fault. (**e**) Silicified brecciated limestone with chalcedony cement in large NE–SW fault adjacent to the quarry (see inset to (**a**)). (**f**) A 15 m long × 10 m high fully exposed planar NW–SE fault surface with 1–2 cm thick veneer of fluorite (inset).

cutting relationships between the fault pairs. These relationships are representative of those seen across the NPO in the Alston Block; the only exceptions occur in those cases where the Phase 1 faults are locally reactivated during Phase 2 (see below).

Quarter Point veins

The abandoned West Rigg opencut [NY9112239208] (Fig. 4a and b) is located 1 km north of the village of Westgate. The exposures here

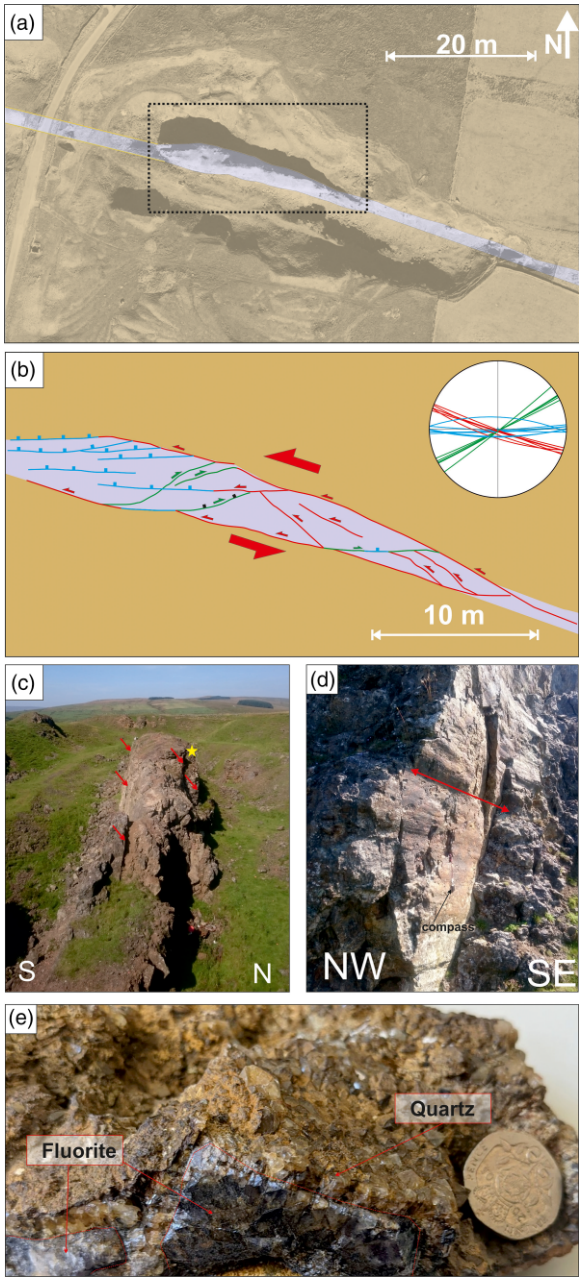

Fig. 4. (**a**) Aerial view of West Rigg Quarry (©Getmapping 23 August 2015 using EDINA Aerial Digimap Service) with the fluorite–quartz–galena-bearing Slitt Vein highlighted in purple. Dashed black box indicated location of map in (**b**). (**b**) Detailed map and stereoplot of shear plane sets exposed in Slitt Vein: east–west normal (blue), NE–SW dextral (green) and WNW–ESE sinistral (red). (**c**) View of the central quartz-rich stockwork of the Slitt Vein with subvertical fault surfaces (red arrowed). (**d**) Subhorizontal corrugations on a NW–SE fault surface. (**e**) Early fluorite crystals (purple) overgrown by euhedral quartz with iron staining (brown). Location of sample is shown by yellow star in (**c**).

within the Carboniferous Great Limestone offer an unprecedented opportunity to view an example of the North Pennine vein systems in three dimensions (Fig. 4c–e). The quarry extracted 'limonitic' ironstone formed by the supergene alteration of extensive siderite and/or ankerite replacement deposits within the limestone adjacent to the Quarter Point Slitt Vein. Narrow abandoned stopes, formerly worked underground for lead ore, may be seen in the centre of the otherwise barren quartz–fluorite stockwork, which stands as a prominent rib that extends for *c.* 80 m through the centre of the quarry (Dunham 1990; Bevins *et al.* 2010). Here the vein strikes on average towards 120°, but internally contains three sets of interconnected shear planes: east–west normal faults, NW–SE sinistral faults and NE–SW dextral faults (Fig. 4b). These slip surfaces are associated with polished and striated surfaces and mineralized breccias (Fig. 4c and d) indicating that fault activity and mineralization were synchronous. The kinematics of these fault sets within the Slitt Vein suggests that the whole system represents a sinistral transtensional brittle shear zone (Fig. 4b). As with almost all NPO veins, no definitive order of mineralization is observed at this location, but large fluorite crystals are commonly overgrown by crusts of euhedral quartz crystals or siderite (Fig. 4e; Dunham 1990). The commonly euhedral forms of the crystals in the vein array suggest that the fluids were often precipitated in open voids probably as a consequence of the extensional or dilatational and relatively near-surface nature of the fault zone deformation (e.g. Woodcock *et al.* 2014).

The Great Sulphur Vein (GSV) is a 12 km long (at surface), broadly WNW–ESE-trending structure composed of a stockwork of numerous smaller, structurally controlled veins (Dunham 1990). It attains a maximum width of 365 m, but appears to narrow downward and may represent the root zone for the Quarter Point vein system (Bevins *et al.* 2010). A characteristic feature of the GSV is a marked vertical zonation in which quartz, both as pure ribs and as extensive replacements of limestone, mudstone and sandstone, dominates an upper zone, beneath which there appears to be a more or less continuous sulfide-rich zone in which abundant pyrite, marcasite and pyrrhotite are locally accompanied by chalcopyrite (Dunham 1990). Galena, sphalerite and fluorite are generally scarce, but occur in local concentrations.

A sulfide-rich portion of the GSV is exposed in the River South Tyne near Sir John's Mine at Tynehead [NY76043756]. Here the vein is hosted within the Tynebottom Limestone where metasomatism has resulted in almost complete quartz replacement in areas up to 10 m wide, indicating a significant interaction between the vein-hosted fluids and the Carboniferous wall rocks. An east–west-striking sinistral oblique normal fault exposed below a small waterfall is surrounded by a series of small subvertical veins composed mostly of quartz, with smaller amounts of pyrite and chalcopyrite. These veins range from 10 cm to 1 mm in width, with the larger veins carrying the majority of the sulfides. NE–SW veins are associated with local brecciation and cataclasis whereas associated north–south- or east–west-striking veins are dominated by mode 1 tensile opening.

Regionally, the ESE–WNW (Quarter Point) vein fractures are characterized by abrupt changes of strike. Where the orientation is ESE–WNW, as at West Rigg, they are commonly poorly mineralized or barren. Where they assume an almost east–west orientation, as at Tynehead, they typically carry wide (locally up to >10 m) mineralized orebodies. This is consistent with their sinistral transcurrent displacement, as recognized by Greenwood and Smith (1977) and was an important factor in the successful location and working of major fluorite orebodies at several mines during the twentieth century.

Lead Veins

In the bed of the River South Tyne at Garrigill, the ENE–WSW-trending Browngill Vein [NY74364181] is exposed cutting silicified Tynebottom Limestone wall rocks (Dunham 1990). This is a typical example of one of the Lead Veins, which typically contain varying amounts of quartz, galena, pyrite, marcasite, chalcopyrite and sphalerite. The majority of the mineralization at Garrigill occurs within a series of NE–SW-trending veinlets up to 15 cm wide, which are composed primarily of quartz, galena and marcasite. Brecciation of both veins and host rocks is commonly associated with the thicker veins, with small dextral dilatational jogs well preserved along associated smaller veins with the same trend.

The Old Moss Vein is one of several NE–SW-trending veins formerly worked underground from Park Level Mine (now Killhope Lead Mining Museum). It is exposed within the Great Limestone in the bed and north bank of Killhope Burn *c.* 700 m upstream from the museum [NY82044334]. The vein is here up to 1 m wide and comprises NE–SW-trending bands composed of abundant galena and a little sphalerite in a matrix of dark brown partially oxidized siderite and ankerite. The limestone adjacent to both sides of the vein is replaced for up to around 2 m by dense crystalline ankerite and siderite in which small vugs, locally in bedding-parallel bands, are lined with fluorite, quartz and galena (Dunham 1990; Bevins *et al.* 2010). No definite sense of shear is preserved here.

Cross Veins

The Browngill Vein seen at Garrigill can be traced for *c.* 5 km eastward from its junction with the NNW–SSE-trending Lee House Well Vein [NY72704140] to Nenthead. Unlike most of the NNW–SSE Phase 1 fractures across the orefield, the numerous members of this set around Nenthead are unusual both for their richly mineralized fillings and for extensive replacement deposits associated with the development of 'flats' in the Great Limestone. The absence of both fluorite and barium gangue minerals is a notable feature of these deposits.

Examples of these flats are well exposed in the waterfall in the River Nent [NY78644299] where original bedding, joints, stylolites and some fossils are replaced by hard crystalline ankerite and quartz with abundant galena and sphalerite and minor amounts of pyrite filling small veinlets and vugs within the altered rock. Limestones exposed in the river gorge downstream of the waterfall exhibit numerous vertical NE–SW-trending minor joints, some of which exhibit ankerite and quartz mineralization along NE–SW-trending joints (Dunham 1990; Bevins *et al.* 2010). The main mineralized structures exposed here are subvertical NW–SE dextral strike-slip faults. A second set of subvertical north–south-trending tensile veins filled by ankerite and minor amounts of galena are consistent with the inferred dextral movement along the adjacent NW–SE faults.

Inversion structures, southern margin of the Alston Block

The Lunedale Fault forms the southern bounding fault of the Alston Block (Fig. 1a and b) and, although outside the 'fluorite zone' that is the focus of this study, the structures found therein are of importance for understanding the regional structural history of the North Pennines and its associated mineralization. The main fault is a poorly exposed, steeply southward-dipping, east–west-trending structure with an along-strike length of roughly 20 km (Dunham 1990), which separates the Alston Block from the Stainmore Trough (Fig. 1a inset). The Lunedale Fault and related structures and associated mineralization are exposed at the disused Closehouse Mine [NY85252275] (Fig. 5a). The host lithologies here are Carboniferous limestones and sandstones of the Alston Formation, together with dolerite of the Whin Sill dyke emplaced here within the Lunedale Fault (Dunham 1990; Bevins *et al.* 2010). Two sets of unmineralized joints trend north–south and east–west and are probably related to the regional set of jointing observed throughout the NPO. The structure of the area is dominated by an *c.* 100 m wide, east–west-striking anticline (Fig. 5a and b) cross-cut by a series of mostly southward- and subordinate northward-dipping thrust faults that have been infilled by later quartz mineralization (Fig. 5b and c). Slickenlines preserved on the thrust faults indicate a dip-slip reverse shear sense (Fig. 5a) with offsets that are mostly small (<1 m). Slickenline-bearing bedding planes are also common

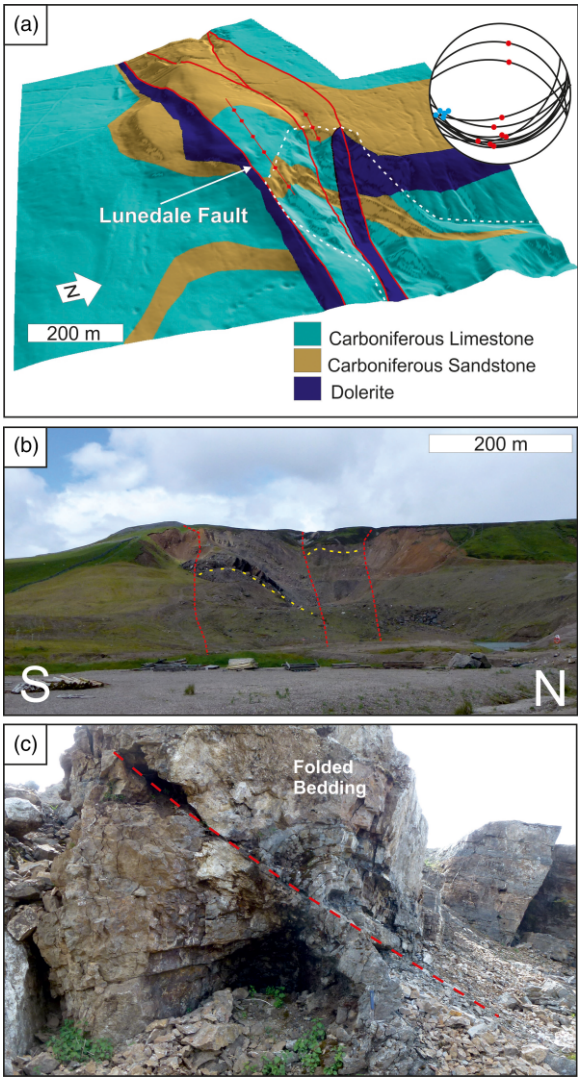

Fig. 5. (**a**) Geological map of Closehouse mine draped over a DEM (©Environmental Agency using EDINA Lidar Digimap Service) showing the main structures (faults, folds) and relationship to the associated dolerite intrusions. The edge of the current mine workings is shown by white dashed line. Stereoplot shows shallow-plunging fold hinges (blue) and thrust planes with slickenlines (red). (**b**) View of Closehouse mine looking west with the main faults highlighted in red and the associated antiformal structures in yellow. (**c**) Antithetic north-dipping thrust fault within the Carboniferous limestones with hanging-wall anticline.

and appear to be related to flexural slip during folding rather than fault motion. To the north of this structure, a *c.* 20 m wide fault-bounded slice is exposed containing a gently west-plunging anticline–syncline pair (Fig. 5a and b). The bounding faults have shallowly plunging slickenlines consistent with sinistral-oblique reverse movement. To the south of the main fold, outcrop-scale antithentic thrusts and associated anticlines are exposed within the limestone (Fig. 5c).

Closehouse Mine is significant for its exposure of an east–west-striking altered, dolerite dyke thought to be a feeder to the nearby Whin Sill (Fig. 5a; Dunham 1990; Bevins *et al.* 2010), although the importance of these 'feeder' dykes with regard to magmatism and the associated magmatic fluids is now open to some dispute. Robinson (2020) has proposed a emanative centre for the Whin Sill located close to Cow Green Reservoir [NY8136129014] some distance from the horst-bounding structures seen at Closehouse Mine.

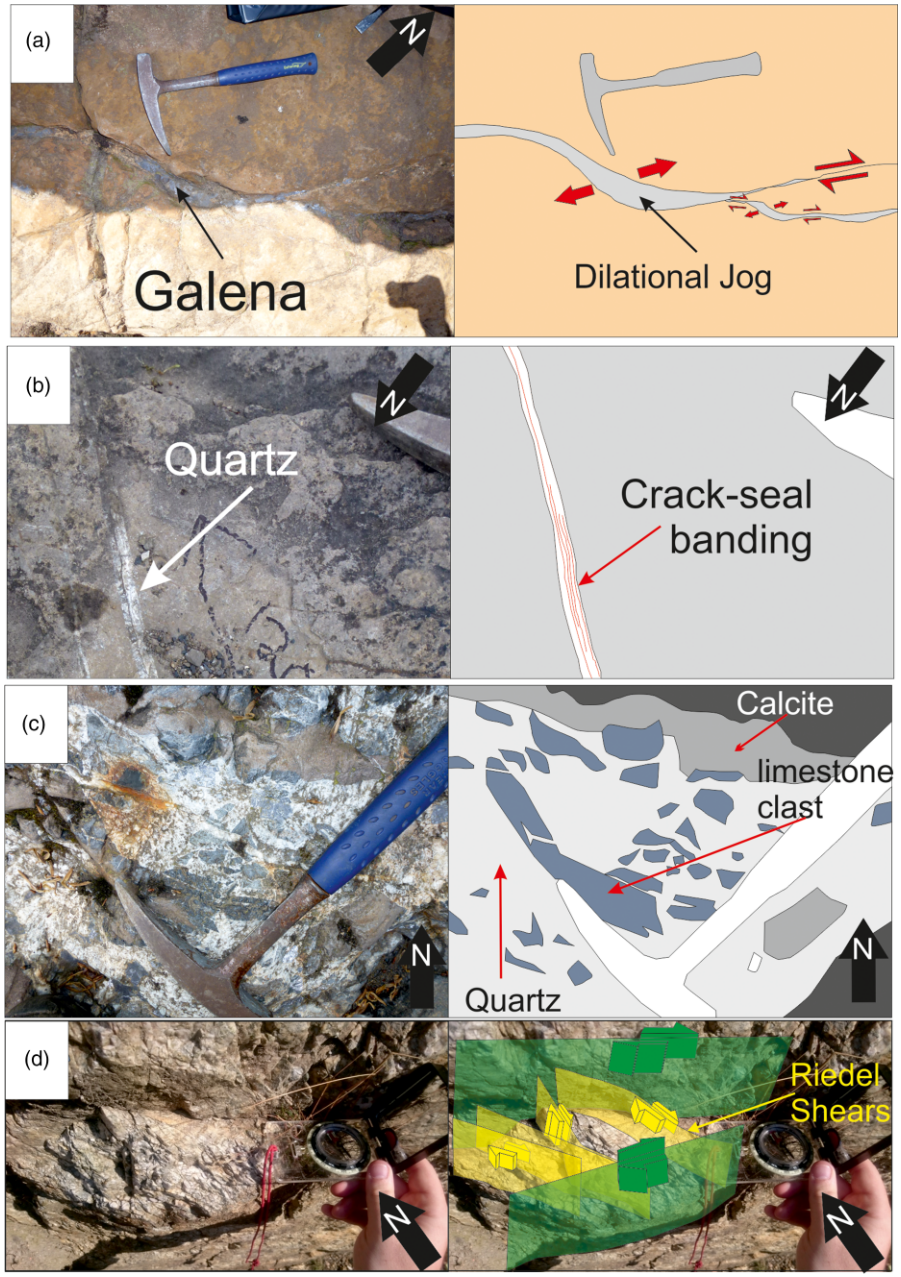

Fig. 6. The four main outcrop-scale vein types observed within the NPO. (**a**) Massive monomineralic to polymineralic veins with local dilational jogs indicating shear sense associated with mineralization. River Nent section, Nenthead [NY78644299] (Cross Vein set). (**b**) Tensile (Mode I) veins ± crack seal banding. South Tyne River section, Tynehead [NY76043756] (Quarter Point vein set). (**c**) Mineralized breccia containing clasts of wall rock (commonly silicified) and brecciated vein material. South Tyne River section, Garrigill [NY74364181] (Lead Vein set). (**d**) Brecciated fluorite mineralization (white) cut by dextral strike-slip faults (green) and associated Riedel shears (yellow). West Rigg quarry [NY91123921] (Quarter Point set).

Petrology and microstructures

Mineralized fractures (faults, veins) in the NPO range in width from millimetres to metres and in length from 1 m to to many kilometres. The largest of the Quarter Point veins (Slitt Vein, Great Sulphur Vein, Red Vein) are in excess of 10 km long and 10 m wide. Three main styles of mineralized fracture fills are recognized.

(1) Simple tensile or hybrid veins, with slickenlines well developed in strike-slip segments and asymmetric jogs or pull-aparts in more tensile segments, both of which are useful as kinematic indicators. These veins are monomineralic or occasionally bimineralic, with pods of sulfide mineralization intergrown with gangue material (Fig. 6a).

(2) Mode I tensile veins with crack-seal textures that can be either monomineralic or polymineralic with common compositional banding (Fig. 6b).

(3) Breccia (± minor cataclasis) where all phases of mineralization are present intergrown within a brecciated wall rock fill (Fig. 6c). Slickenlines, Riedel shears and the orientation of associated second-order tensile veins are common kinematic indicators (Fig. 6d). In general, clay gouges were not observed in surface exposures, but are very occasionally observed in underground mine workings. This may reflect the poor preservation potential of such fault rocks or may be due to the relatively minor displacements along many of the structures present.

Examination of thin sections and hand specimens collected for this study reveals that, as established by Dunham (1934), fluorite, quartz, galena, sphalerite, pyrite, marcasite, pyrrhotite, siderite, ankerite and chalcopyrite are the dominant minerals within the orefield's central fluorite zone, with barium minerals (e.g. barite, witherite) taking the place of fluorite and quartz in the outer barium zone. Pyrite and marcasite appear to be widespread, although in generally modest amounts, throughout the sampled mineralization, with greater concentrations of these and with the addition of pyrrhotite, chalcopyrite and locally very small amounts of bismuth and cobalt minerals in earlier phases of mineralization.

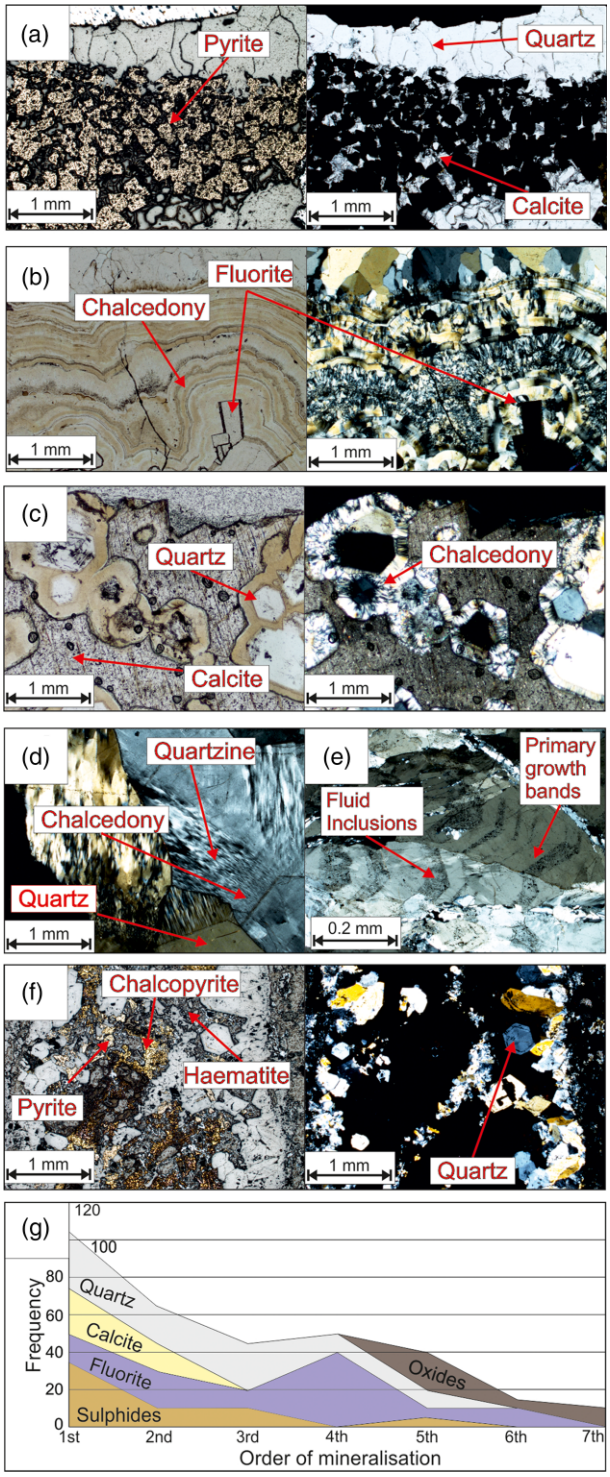

Fig. 7. Photomicrographs of primary growth textures in veins of the NPO. (**a**) Massive monomineralic to polymineralic veins (in this case, pyrite, calcite and quartz) with euhedral to subhedral crystal habits. Sample from Nenthead [NY7864442992] (NNW–SSE Cross Vein). (**b**) Crustiform to colloform mineralization (chalcedony) with overgrowths of euhedral crystals (fluorite). Sample from Groverake Mine [NY9037044138] (ESE–WNW Quarter Point vein). (**c**) Cockade or moss veins with zoned spheroids (quartz with chalcedony overgrowths) 'floating' in a matrix (calcite). Sample from Groverake Mine [NY9037044138] (ESE–WNW Quarter Point vein). (**d**) Phase transition growth of related mineral phases; in this case quartz crystals are overgrown by crystals that start as chalcedony and evolve into quartzine before finally growing as quartz. Sample from Tynehead [NY7603737549] (ESE–WNW Quarter Point vein). (**e**) Primary growth zonation is often visible in quartz (as in this case), fluorite and calcite. This is usually highlighted in optical images by the presence of fluid inclusions or impurities (often microsulfides). Sample from Tynehead [NY7603737549] (ESE–WNW Quarter Point vein). (**f**) Euhedral quartz with a matrix of anhedral, intergrown metalliferous ore minerals (pyrite, chalcopyrite, hematite). Sample from Groverake Mine [NY9037044138] (ESE–WNW Quarter Point vein). (**g**) Stacked frequency chart showing the order of mineralization observed in thin section analysis of samples collected from the fluorite zone of the Alston Block. Although most phases are seen to be coeval (with the exception of oxide or supergene minerals) it should be noted that calcite and the metalliferous sulfides (pyrite, chalcopyrite, marcasite, galena) are generally earlier. In (**a**)–(**c**) and (**f**), left-hand images are in plane-polarized light (ppl), whereas right-hand images are in crossed-polars. Images (**d**) and (**e**) are both in crossed-polars.

The abundance of iron minerals within these early assemblages (Fig. 6e), together with the widely observed occurrence of iron metasomatism of limestone wall rocks adjacent to vein fractures of all orientations across the orefield, indicates that iron was a significant and major component of the earliest mineralizing fluids. Occurrences of magnetite, of metasomatic origin, recently reported from the contact zone of the Whin Sill in Upper Teesdale (Young 2017), together with the abundance of magnetite within unique nickel-bearing skarn-type mineralization associated with the Teesdale Fault (Young *et al.* 1985), are further evidence of early iron-rich mineralizing fluids.

Microstructurally, a huge array of vein textures are preserved within the NPO (Fig. 7a–f). Primary crystallization fabrics throughout the orefield include massive veins (Smirnov 1954) and crustiform (Adams 1920), colloform (Rogers 1917), comb (Boyle 1979) and zonal (Smirnov 1954) types; these findings suggest that the surface-exposed veins retain their original textures and chemistry. Crack-seal textures (both syntaxial and antitaxial) are also widely observed (e.g. Fig. 6b). Deformation fabrics within the mineralized faults of the NPO are dominated by the presence of mineralized breccias (Fig. 8a–e). These breccias commonly record multiple deformation and mineralization events where clasts of fractured or brecciated material are incorporated into subsequent veins or breccias of similar composition (e.g. Fig. 8c); in other cases, brecciated mineral fills are cross-cut by compositionally similar veins (Fig. 8b and d). The cyclical nature of these breccias where vein material has been brecciated, healed and then re-brecciated, or cross-cut by further veining, is indicative of syntectonic mineralization following hydrofracturing events. The local preservation of cockade textures and open vugs also suggests that, in some cases, fractures were incompletely sealed and cemented, allowing repeated periods of fluid flow (Frenzel and Woodcock 2014).

Recrystallization (feathery, flamboyant and ghost-sphere; Adams 1920) and replacement textures (ghost-cubes and skeletal crystals; Morgan 1925) are commonly preserved, showing that not all veins have retained their primary mineralogy and fabric (Fig. 9a–c). Fluorite microstructures in particular suggest that significant amounts of remobilization and healing or reprecipitation have occurred; for example, replacement of fluorite by quartz or chalcedony (Young and Hopkirk 2019). Within fluorite crystals, multiple generations of fluid inclusions are observed. These fluid inclusions highlight the presence of growth zoning and pervasive healed microfractures (Fig. 8e). Optical cathodoluminescence (OCL) shows that recrystallization or healing of fluorite breccias is widespread, illustrating that this mineral is especially prone to dissolution and reprecipitation with overgrowth showing perfect optical continuity (Fig. 10a). By contrast, dissolution and precipitation with optical continuity is not observed in calcite crystals, where the textures revealed by OCL are more consistent with those observed using conventional optical microscopy (Fig. 10b).

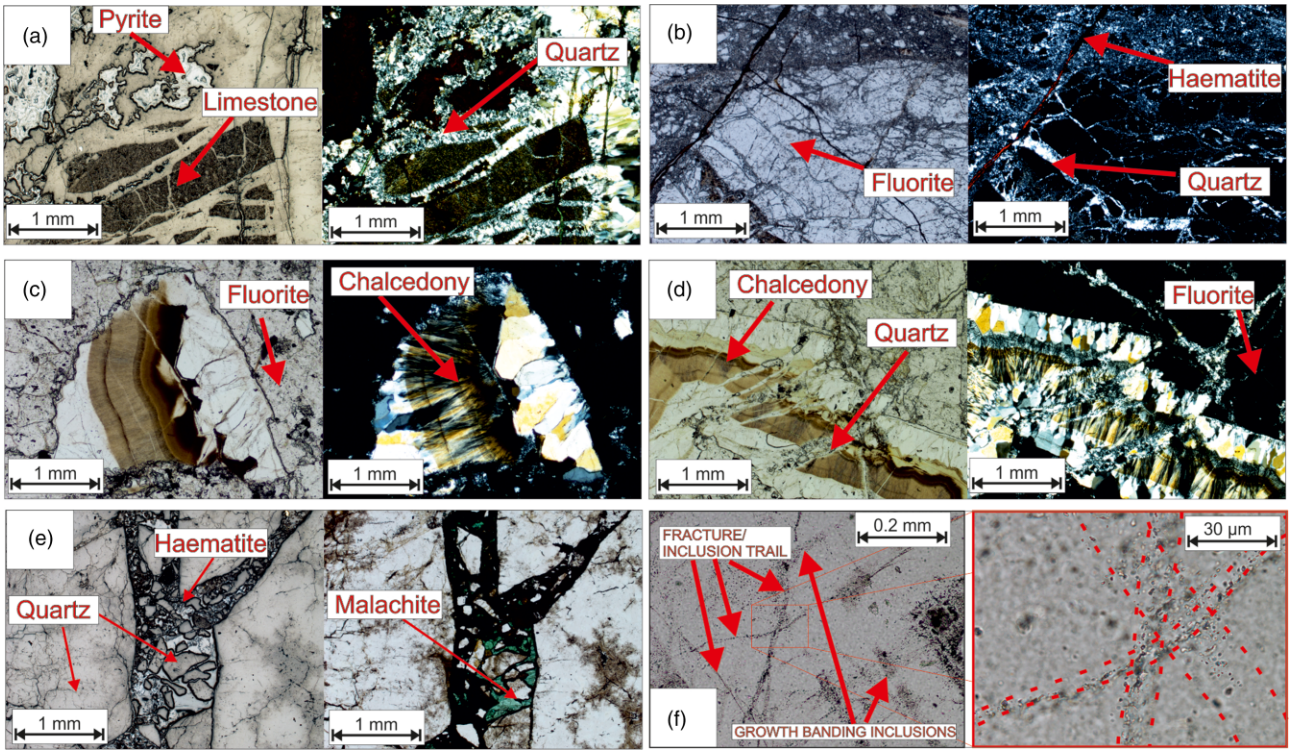

Fig. 8. Photomicrographs of deformation textures observed in mineralized faults of the NPO. (**a**) Jigsaw-brecciated fragments of limestone wall rock cemented by intergrown quartz and pyrite. It should be noted that brecciation in this case was potentially explosive and related to transient high fluid pressures rather than to shear or attrition. Sample from Westernhope [NY9203934556] (ENE–WSW Quarter Point vein). (**b**) Pervasive microfracturing in fluorite clast (lower part of image) suspended within a hematite-cemented fluorite cataclasite (upper part of image). Sample from Westrigg [NY9115139186] (ESE–WNW Quarter Point vein). (**c**) Clast of vein material (chalcedony, quartz) suspended in a fluorite matrix. Sample from Sedling [NY8592241110] (ESE–WNW Quarter Point vein). (**d**) Alternating bands of crustiform chalcedony and fluorite offset by microfractures and quartz microveins. Sample from Sedling Mine [NY8591241093] (ESE–WNW Quarter Point vein). (**e**) Fractured quartz vein cross-cut by microbreccia cemented with oxides and malachite. Sample from Westernhope [NY9203934556]. (**f**) Healed microfracturing in quartz grains with fluid inclusions (Tuttle lamellae); right-hand image shows a higher-power view. Sample from Tynehead [NY7603737549] (ESE–WNW Quarter Point vein). In (**a**) and (**f**), left-hand images are in reflected light, whereas those in (**b**)–(**d**) and (**e**) are in ppl. Right-hand images in (**a**)–(**d**) are in crossed polars, whereas those in (**e**) and (**f**) are in ppl.

Results

Stress inversion analyses

Stress inversion analysis was carried out using all data collected from slickenline-bearing faults and fractures of the Alston Block of the NPO. Field observations at locations such as Bollihope Quarry clearly show that there are two sets of structures developed: an earlier set of Phase 1 NNW–SSE and NNE–SSW faults and fractures and a younger cross-cutting population of Phase 2 ENE–WSE and ESE–WNW structures. Misorientations resulting from block rotations and gentle folding in the Alston Block are negligible. A stress inversion analysis of the earlier NNE–SSW and NNW–SSE faults suggests that they are related to north–south shortening in a contractional reverse faulting or transpressional regime (σ_3 vertical, Fig. 11a). The younger and more widespread ESE–WNW and ENE–WSW fault sets related to Phase 2 yield north–south extension and east–west shortening consistent with a strike-slip or transtensional regime (σ_2 vertical, Fig. 11b). The Mohr circle analysis of the earlier NNE–SSW and NNW–SSE Phase 1 structures (highlighted in green) shows they are highly misoriented, which suggests that in areas where they have been locally reactivated (e.g. Nenthead) elevated

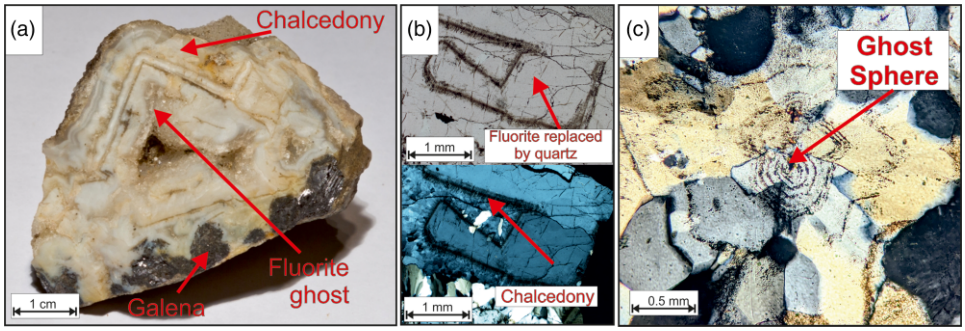

Fig. 9. Replacive mineral textures within the NPO. (**a**) Hand-specimen of fluorite replaced by silica. Sample from Shildon Mines, Blanchland, Northumberland [NY96255080] (NE–SW Lead Vein). (**b**) Fluorite replaced with quartz with relict grain boundary still visible as a band of chalcedony or feathery quartz. Upper image in ppl; lower image in crossed polars. Sample from Redburn, Rookhope [NY9328343072] (ESE–WNW Quarter Point vein). (**c**) 'Ghost spheres' are commonly observed replacement texture. Here cockade or moss textures are replaced by silica with optically continuous crystals overgrowing the original texture; Sample from Redburn, Rookhope [NY9328343072] (ESE–WNW Quarter Point vein).

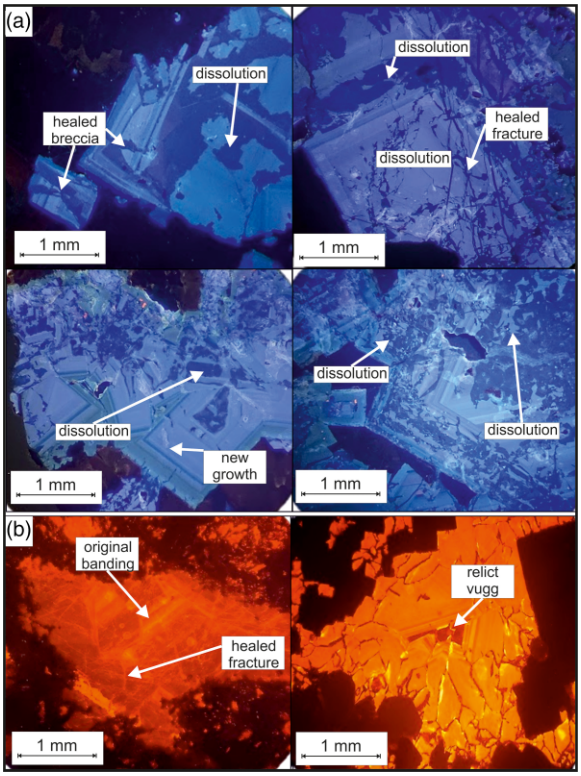

Fig. 10. (**a**) Optical cathodoluminescence (OCL) images of fluorite crystals showing multiple dissolution, precipitation and brecciation events that are not visible using traditional optical microscopy. Samples from Sedling mine [NY8592241110] (ESE–WNW Quarter Point vein). (**b**) OCL images of calcite crystals showing zonal growth and brecciation, but lacking the obvious dissolution–precipitation textures seen in fluorite. Samples from Nenthead [NY7864442992] (ESE–WNW Quarter Point vein)..

pore fluid pressures would have been required locally during mineralization.

Re–Os geochronology

The total Re and Os abundances of pyrite range from 3.5 to 228 ppt and from 1 to 45 ppt (Table 1), respectively. The $^{187}Re/^{188}Os$ and $^{187}Os/^{188}Os$ ratios range from 0.6 to 97.6 and from 0.12 to 0.63, respectively, with the exception of sample RO572-4_BG5A, which displays $^{187}Re/^{188}Os$ and $^{187}Os/^{188}Os$ ratios of 682.2 and 3.7 (Table 1). To account for the uncertainties between the $^{187}Re/^{188}Os$ and $^{187}Os/^{188}Os$ data we present the latter with the associated uncertainty correlation value, rho (Ludwig 1980), and the 2σ calculated uncertainties for $^{187}Re/^{188}Os$ and $^{187}Os/^{188}Os$ (Table 1). The regression of all the Re–Os data using IsoplotR (Vermeesch 2018) and the ^{187}Re decay constant (λ) of $1.666e^{-11} \pm 5.165e^{-14}$ a^{-1} (Smoliar *et al.* 1996) yielded a Model 3 Re–Os date of 311.6 ± 19.8 (6.4%) Ma, with an initial $^{187}Os/^{188}Os$ of 0.15 ± 0.01 (2σ, mean squared weighted deviates (MSWD) = 0.98; Fig. 12a).

The significant uncertainty in the calculated Re–Os date (6.4%) is due to the low total concentrations of Re and Os in the pyrite and the scatter exhibited in the best-fit of the Re–Os data as indicated by the MSWD value of 0.98. Calculation of initial $^{187}Os/^{188}Os$ ratio at 312 Ma indicates the presence of two outlying samples (CB10 and TH1), which have a slightly more radiogenic composition (0.34 ± 0.11 and 0.38 ± 0.11, respectively; Fig. 12b), that ultimately cause scatter about the line of best-fit of the Re–Os data. Regression of the remaining Re–Os data, excluding CB10 and TH1, yielded a Model 1 Re–Os age of 304 ± 20 (6.5%) Ma with a significantly lower MSWD of 0.14 and an initial $^{187}Os/^{188}Os$ ratio of 0.15 ± 0.01 (7.9%) (Fig. 12c).

The Re and Os abundances of the Whin Sill sample are 472 ppt and 2 ppt, respectively. The $^{187}Re/^{188}Os$ and $^{187}Os/^{188}Os$ ratios are 4754.2 ± 531.5 and 23.193 ± 1.444, respectively. Based on the geochemistry and petrology, the sill is probably mantle-derived (Thorpe and MacDonald 1985); as such an initial $^{187}Os/^{188}Os$ ratio of 0.12 ± 0.01 was assumed to calculate a model Re–Os date. On the basis of an initial $^{187}Os/^{188}Os$ ratio of 0.12 ± 0.01 (Permian mantle $^{187}Os/^{188}Os$ composition calculated from Meisel *et al.* 1996) a Re–Os date of 290.2 ± 29 Ma was calculated. The latter also indicates that the Os budget in the Whin Sill sample is 99.5% radiogenic ^{187}Os.

Discussion

A new structural model for the North Pennine Orefield

The four regionally pervasive fault orientations observed within the NPO (Dunham 1990) can be grouped into two broad populations based on observed cross-cutting relationships (Fig. 13a and b): Phase 1 consists of NNW–SSE faults (tensile and mostly dextral) and NNE–SSW faults (sinistral) with associated small-scale north–south-trending (<50 cm wide) tensile veins; Phase 2 consists of ESE–WNW faults (normal, tensile and sinistral) with ENE–WSW faults (dextral and tensile), which are commonly associated with larger (<5 m wide) east–west striking vertical tensile veins.

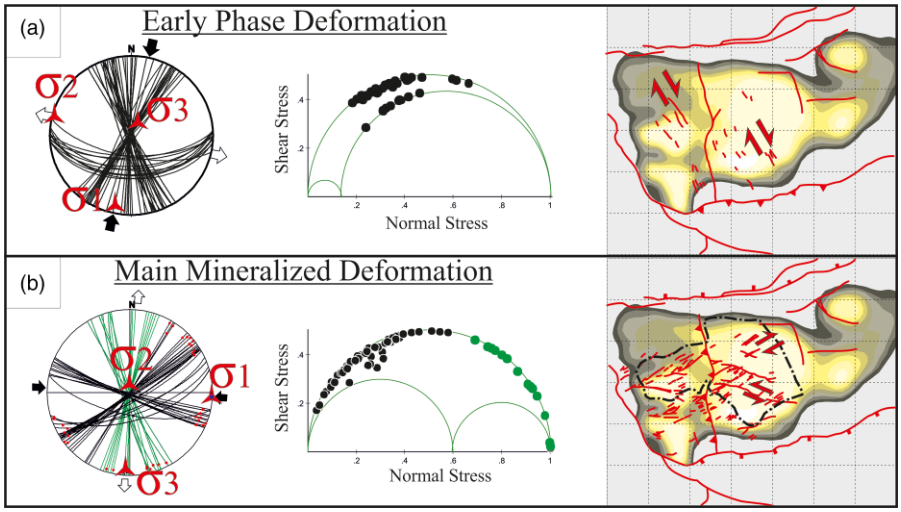

Fig. 11. Stereoplots with stress inversion analyses, Mohr circle plots and maps for all slickenline-bearing structures of the NPO for (**a**) Phase 1 and (**b**) Phase 2 structures. These suggest that Phase 1 was a reverse faulting regime with north–south shortening consistent with far-field Variscan inversion, whereas Phase 2 was a strike-slip or transtensional regime with north–south extension and east–west shortening. The green planes on the stereonet and points on the Mohr diagram correspond to mineralized faults interpreted to have been formed during the earlier phase of deformation that have been reactivated during the main phase of mineralization. The position of these planes on the Mohr diagram shows that these structures are unfavourably oriented for slip. See text for further details.

Table 1. *Synopsis of the Re and Os pyrite data from the sulfide-bearing veins and Whin Sill of the Alston Block*

Batch or sample	Re		Os		$^{187}Re/^{188}Os$	±	$^{187}Os/^{188}Os$	±	rho	Os_i							
	(ppt)	±	(ppt)	±						308 Ma	±	297 Ma	±	295 Ma	±	290 Ma	±
RO579-1_NHM1b	42.2	3.9	0.9	0.1	260.3	58.6	1.43	0.32	0.832	0.17	0.03	0.23	0.04	0.24	0.04	–	–
RO550-8_S3	15.8	3.9	35.3	1.2	2.2	0.6	0.16	0.02	0.216	0.15	0.02	0.15	0.02	0.15	0.02	–	–
RO572-1_SJM2	63.8	4.0	3.4	0.1	97.6	11.2	0.63	0.08	0.627	0.12	0.01	0.15	0.01	0.15	0.01	–	–
RO572-4_BG5A	227.8	4.1	2.4	0.1	682.2	86.6	3.73	0.56	0.832	0.19	0.02	0.34	0.03	0.37	0.04	–	–
RO572-5_S1	3.5	4.0	1.0	0.1	17.5	20.5	0.27	0.07	0.105	0.18	0.11	0.18	0.11	0.18	0.11	–	–
RO572-6_S2	5.9	4.0	45.7	1.6	0.6	0.4	0.16	0.02	0.082	0.16	0.05	0.16	0.05	0.16	0.05	–	–
RO572-7_TH1	7.8	4.0	1.1	0.1	36.9	19.8	0.57	0.12	0.262	0.38	0.11	0.39	0.11	0.39	0.11	–	–
RO572-9_CB10	7.0	4.0	1.1	0.1	31.1	18.5	0.50	0.10	0.222	0.34	0.11	0.35	0.11	0.35	0.11	–	–
RO590-2_CBWH1	472.4	47.8	1.9	0.1	4754.2	531.5	23.19	1.44	0.324	–	–	–	–	–	–	0.15	0.01

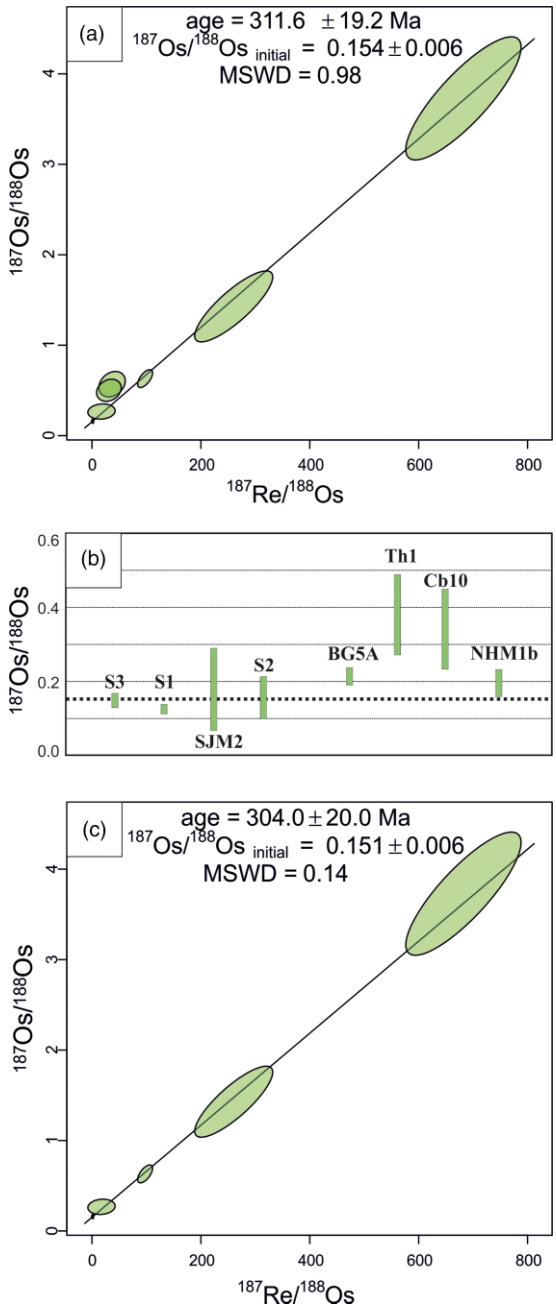

Fig. 12. (**a**) Re–Os isochron for all eight samples collected from the NPO yielding a Model 3 age of 311.6 ± 19.2 Ma (MSWD = 0.98) ($^{187}O/^{188}Os$ = 0.154 ± 0.006). (**b**) Initial osmium ratios for all eight samples at 311 Ma showing that samples TH1 and CB10 from peripheral areas of the NPO (Tynehead Th1, Cambokeels CB10) are more radiogenic compared with the other samples. (**c**) Re–Os regression of the North Pennine Orefield with outliers omitted, yielding a Model 3 age of 304 ± 20 Ma (MSWD = 0.14) ($^{187}O/^{188}Os$ = 0.151 ± 0.006).

Stress inversion analyses indicate that the earlier Phase 1 structures are related to north–south shortening, whereas the later Phase 2 structures are related to a superimposed phase of north–south extension and east–west shortening (Fig. 13a and b). The earlier event is consistent with the far-field effects of the Variscan Orogeny during the Late Carboniferous (Warr 2012, and references therein). It led to the sinistrally transpressive inversion of the broadly east–west-striking faults bounding the Alston Block, as evidenced by the reverse faulting and folding observed associated with the Lunedale fault at Closehouse Mine (Fig. 5). It is consistent with an early dextral transpressional movement associated with the Burtreeford Disturbance, dextral shear along the Pennine Fault to

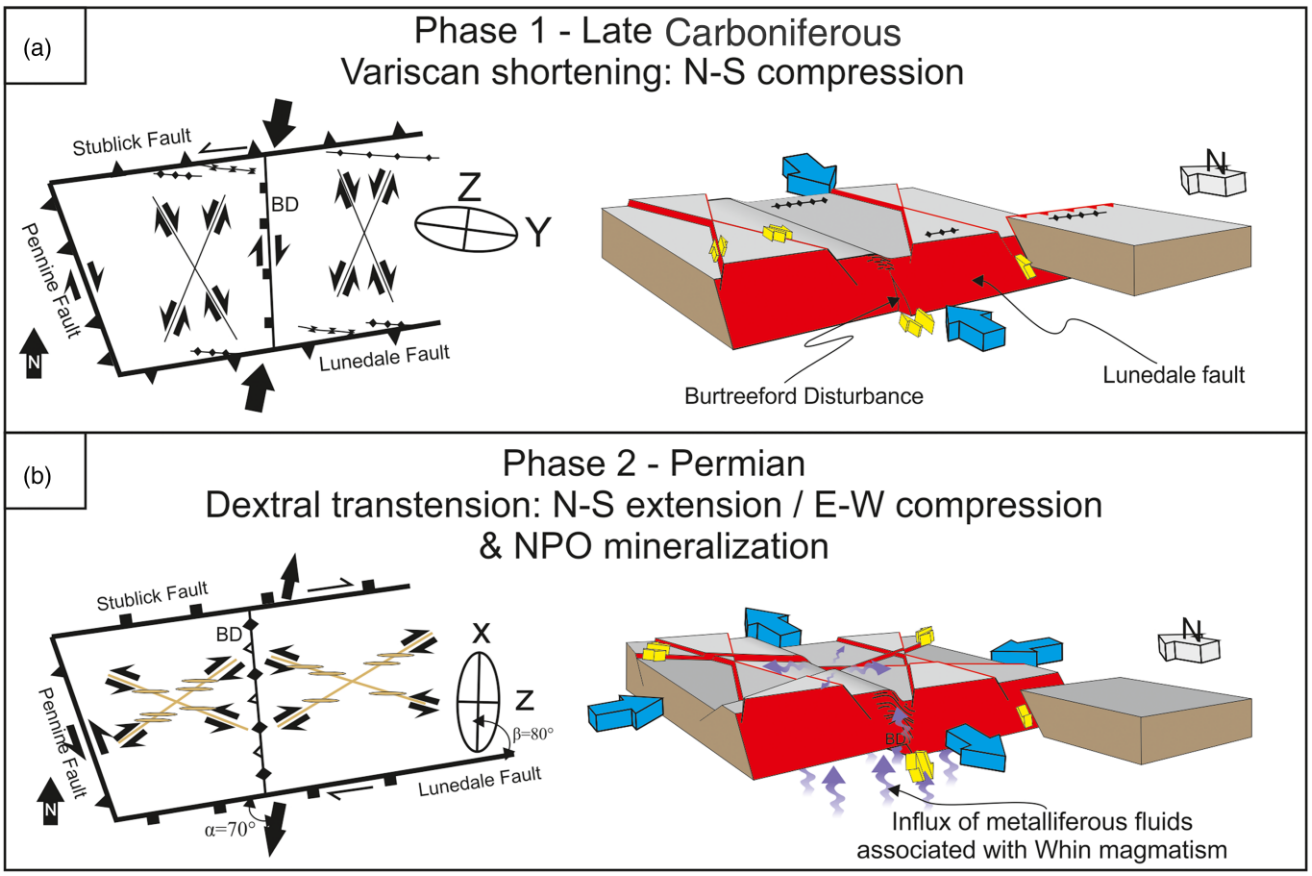

Fig. 13. Map views (left) and 3D models (right) showing the proposed two-stage structural evolution of the NPO. (**a**) Phase 1 deformation owing to north–south Variscan shortening leading to the reverse reactivation and inversion of the surrounding basins and faults bounding the Alston Block, forming east–west folds and thrusts. Within the block, a series of NNW–SSE to NNE–SSW strike-slip faults formed with minor calcite-dominated mineralization and dextral reactivation of the deep-seated Burtreeford Disturbance (BD). (**b**) Phase 2 deformation occurred penecontemporaneously with the emplacement of the Whin Sill at *c*. 297 Ma with north–south extension and east–west shortening reactivating the faults bounding the Alston Block (Stublick and Lunedale faults) as dextral transtensional faults. Within the Alston Block a series of NE–SW to SE–NW strike-slip faults developed and became heavily mineralized by fluids associated with the Whin Sill rising through the orefield close to the Burtreeford Disturbance. As these fluids radiated out from this structure, they interacted with the host Carboniferous rocks and became further enriched, altering their isotopic signature and increasing their economic potential.

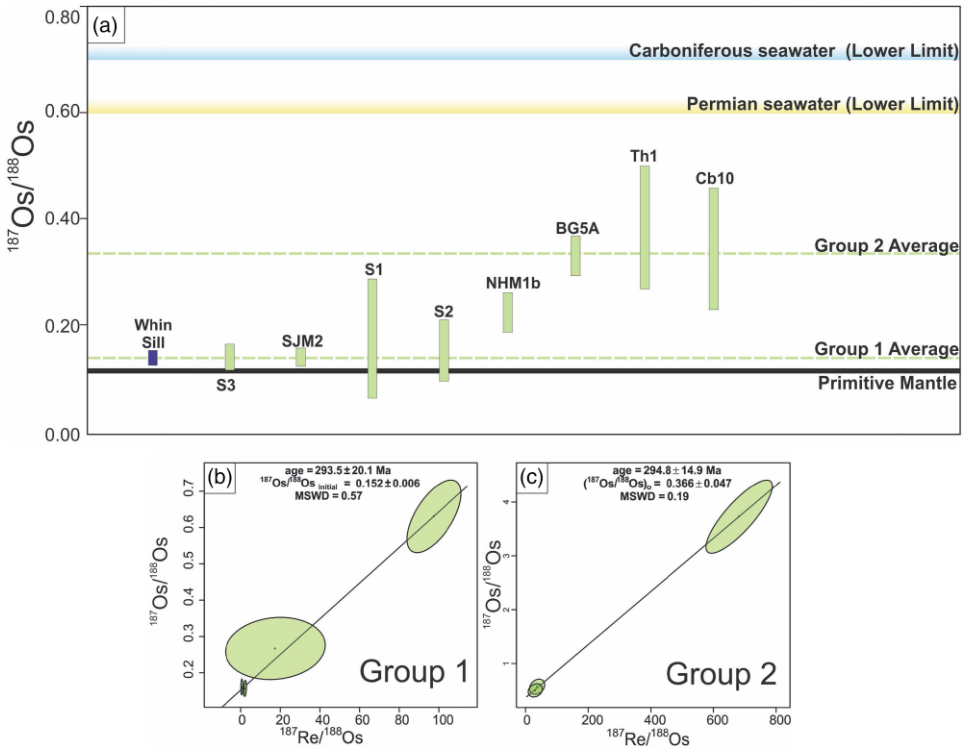

Fig. 14. (**a**) Initial osmium values of sulfide samples collected from the NPO compared with initial osmium ratios for the Primitive Mdntle (black), the Whin Sill (purple), lower limit, Carboniferous seawater (blue) and lower limit, Permian Seawater (yellow). The sulfides can be divided into two groups, with the Group 1 average corresponding to the Whin Sill, whereas Group 2 is slightly more radiogenic. It should be noted that even the most radiogenic samples fall well below the lower limit Carboniferous and Permian values. (**b**) Re–Os regression of Group 1 yielding a Model 3 age of 293.5 ± 20.1 Ma (MSWD = 0.57) ($^{187}O/^{188}Os$ = 0.152 ± 0.006). (**c**) Re–Os regression of Group 2 yielding a Model 3 age of 294.8 ± 14.9 Ma (MSWD = 0.19) ($^{187}O/^{188}Os$ = 0.366 ± 0.047).

the west (Fig. 13a) and also with the late Carboniferous deformation history of the nearby Dent Fault system located further to the south (e.g. Underhill *et al.* 1988; Woodcock and Rickards 2003). In detail, however, the NNE–SSW shortening in the Alston Block lies *c.* 40° clockwise of the NNW–SSE Variscan direction determined in the SW part of the Askrigg Block (Thomas and Woodcock 2015). The faults in the latter area display larger displacements relative to those measured during the present study. Thus the difference in the late Carboniferous shortening in these two areas may reflect a partitioning of broadly north–south orogenic shortening strain between block interiors (North Pennine Orefield) and block margins (Dent–Craven faults), possibly with a component of deep basement control.

The later phase of north–south extension and east–west compression is consistent with the regional dextral transtensional regime (De Paola *et al.* 2005*a*), which is attributed to reactivation of NE–SW Caledonian structures underlying the Northumberland Basin located immediately to the north of the Alston Block. It is suggested that this deformation was synchronous with emplacement of the *c.* 297 Ma Whin Sill and associated intrusions based on observed cross-cutting relationships seen along the Northumberland coastline. This later phase may have led to localized compressional reactivation of the Burtreeford Disturbance, coeval with monoclinal folding and sinistral reactivation of the Pennine Fault to the west (Fig. 13b). Sinistral transtensional reactivation of the Dent Line fault system in the Early Permian is also recognized south of the Alston Block (Underhill *et al.* 1988).

The age and origins of the metalliferous fluids

The Re–Os pyrite data (excluding CB10 and TH1) of the North Pennine Orefield yield a date (304 ± 20 Ma) that overlaps within uncertainty with the timing of emplacement and cooling of the mantle-sourced Whin Sill (U–Pb CA-ID-TIMS baddeleyite, 297.4 ± 0.4 Ma; Thorpe and MacDonald 1985; Hamilton and Pearson 2011). This temporal relationship may indicate that the NPO sulfide mineralization has a direct genetic link to the Whin Sill complex. The Whin Sill as the progenitor of sulfide mineralization of the NPO is further supported by the similarity in the initial $^{187}Os/^{188}Os$ composition of the Whin Sill (*c.* 0.13) and pyrite (*c.* 0.15) (this study).

Considering the temporal and genetic link of the Whin Sill to the NPO mineralization the initial $^{187}Os/^{188}Os$ (Os_i) compositions of pyrite calculated at 297.4 Ma exhibit two distinct populations, Group 1 with a weighted average Os_i of 0.147 ± 0.010 (MSWD = 0.18; S3, SJM2, S1 and S2) and Group 2 with a slightly more radiogenic weighted average Os_i of 0.345 ± 0.030 (MSWD = 0.31; BG5A, TH1 and 496CB10). Sample NHM1b possesses an intermediate Os_i of 0.226 ± 0.04 (Fig. 14a).

The Re–Os data of Group 1 and Group 2 yield Model 1 Re–Os ages of 293.5 ± 20.1 Ma (MSWD = 0.57, Os_i = 0.152 ± 0.006; Fig. 14b) and 294.8 ± 14.9 Ma (MSWD = 0.19, Os_i = 0.366 ± 0.047; Fig. 14c), respectively. The unradiogenic Os nature of the pyrite coupled with the *c.* 294 Ma age strongly supports that Os and by inference ore metals and fluids were derived from the magmatism associated with the Whin Sill Complex. The Re–Os data further illustrate that fluids migrating from the Zechstein Sea (Permian), or simply leaching from the surrounding Carboniferous host rocks and underlying basement (Paleozoic) are all unlikely sources as these would lead to much more radiogenic levels of $Os_i \geq 0.6$. However, the more radiogenic Os_i of Group 2 pyrite and sample NHM1b may represent a slightly more evolved mantle fluid and/or minor inheritance from the surrounding host rocks.

Reported Sm–Nd fluorite data from throughout the NPO were interpreted by Halliday *et al.* (1990) to define no definitive age, but were interpreted to suggest that mineralization occurred between the Carboniferous and Jurassic. The Sm–Nd fluorite data from the Slitt, Groverake and Ferneygill veins collectively yield an errorchron (MSWD = 32) indicating a Late Cretaceous age (Fig.15a). The scatter about the best-fit line is largely caused by the Sm–Nd fluorite data of the Groverake and Ferneygill veins, which independently show considerable scatter in $^{147}Sm/^{144}Nd$–$^{143}Nd/^{144}Nd$ space. Thus, they do not provide any meaningful chronological constraints (Halliday *et al.* 1990).

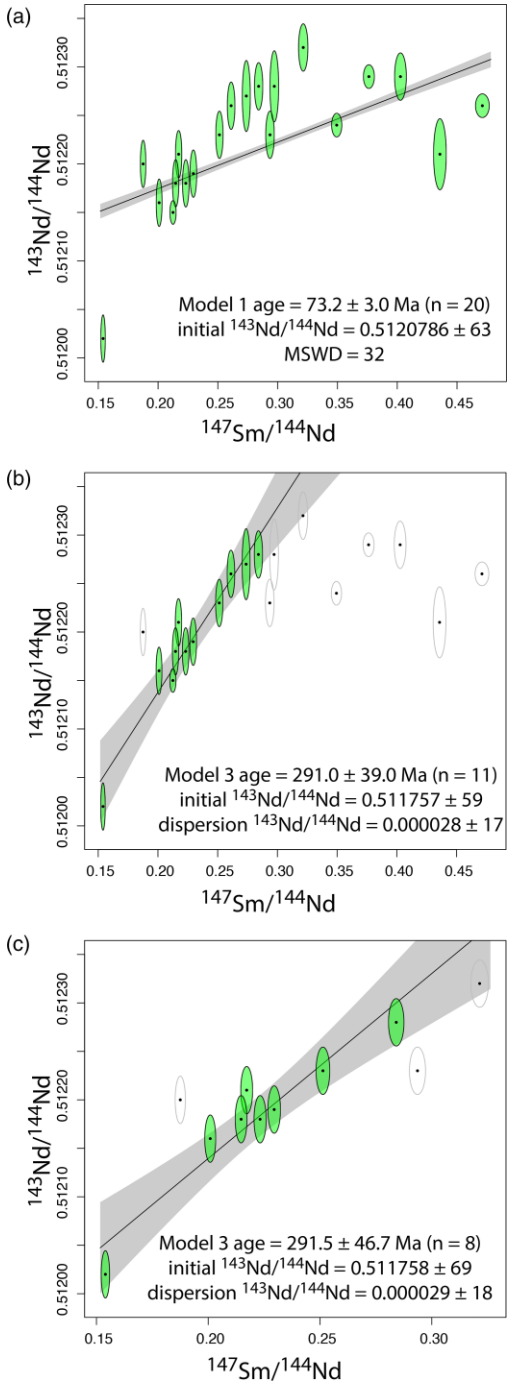

Fig. 15. Sm–Nd fluorite data isochron plots. The Sm–Nd data are from Halliday *et al.* (1990; Table 2). Age calculations were undertaken using IsoplotR (Vermeesch 2018) and a ^{147}Sm decay constant (λ) of 6.524 ± 0.024e^{-12} a^{-1} (Gupta and MacFarlane 1970). (**a**) Errorchron shown for analysis of all Sm–Nd fluorite data from regionally spaced veins (Slitt, Groverake and Ferneygill). (**b**) Sm–Nd plot for samples that possess similar initial $^{143}Nd/^{144}Nd$ values at 295 Ma. (**c**) Sm–Nd plot for only fluorite samples from the Slitt Vein that possess similar initial $^{143}Nd/^{144}Nd$ values at 295 Ma.

Eleven of the 20 fluorite samples (eight of 11 from the Slitt vein, two of four from the Groverake vein and one of five from the Ferneygill vein) possess similar initial $^{143}Nd/^{144}Nd$ compositions at *c.* 295 Ma (the Re–Os age, see above; Table 2). Collectively, the Sm–Nd data for the 11 samples define a Model 3 age of 291.0 ± 39.0 Ma (initial $^{143}Nd/^{144}Nd$ = 0.511757 ± 59, with the scatter defined by a variation in the initial $^{143}Nd/^{144}Nd$ of 0.000028 ± 17 (Fig. 15b). Considering only the Sm–Nd data from the Slitt vein, which roughly corresponds to sample CB10 from Cambokeels of this study, with similar initial $^{143}Nd/^{144}Nd$ at 295 Ma, a Model 1 Sm–Nd age of 293.6 ± 15.7 Ma (MSWD = 5.5) is obtained. Although the best-fit of the Sm–Nd data exhibits some scatter, the age is within uncertainty of both the sulfide mineralization reported in this study and the emplacement of the Whin Sill (Hamilton and Pearson 2011). This is further supported by a Model 3 computation given the degree of scatter about a Model 1 best-fit line to the Sm–Nd data (MSWD = 5.5), which suggests that the deviated scatter is due to geological variations rather than just analytical uncertainty. A Model 3 calculation suggests that the scatter is caused by variation in the initial $^{143}Nd/^{144}Nd$ of 0.000029 ± 18 (age = 291.5 ± 46.7 Ma; initial $^{143}Nd/^{144}Nd$ = 0.511758 ± 69) (Fig. 15c).

The nominal agreement of the Sm–Nd fluorite and Re–Os pyrite chronology suggests a penecontemporaneous relationship with the emplacement of the Whin Sill. Recalculating the εNd for the fluorite, the Whin Sill and the Carboniferous sedimentary rocks (Table 2) at 291.5 Ma, yields values of −9 to −10 for the fluorite, 1.5 for the Whin Sill and −9.8 for the Carboniferous host rocks, which supports a genetic model that invokes leaching of metals from the Carboniferous sedimentary host rocks (Halliday *et al.* 1990; Kraemer *et al.* 2019). This is somewhat at odds with the Os data from the sulfides, but could account for the more radiogenic Os signature observed in Group 2 pyrites (which include sample CB10 from Cambokeels) where interaction with the host rocks and fluid evolution is likely to have occurred.

Alkali magma underplating of the North Pennine batholith associated with the intrusion of the Whin Sill Complex during the earliest Permian has been proposed as the only viable way to account for the observed mineralization (Bott and Smith 2018). This proposal is further supported by REE data from fluorite of the NPO, which display a large europium anomaly indicating that fluorite from this region must have experienced temperatures >250°C (Kraemer *et al.* 2019). This anomaly is absent from the mineralogically similar Askrigg Block and the South Pennine Orefield (Fig. 1a inset) located 40 km and 120 km to the south of the NPO, respectively. The local presence of exotic minerals in the early stages of mineralization in the NPO of the Alston Block alone, such as bismuthinite (Bi_2S_3), synchysite ($CaREE(CO_3)F_2$), argentopentlandite ($Ag(FeNi)_8S_8$), pyrrhotite, cubanite, cosalite ($Pb_2Bi_2S_5$), tungsten-bearing cassiterite, monazite, xenotime, adularia, niccolite and magnetite (Young *et al.* 1985; Ixer *et al.* 1996), has been ascribed to non-'MVT' style mineralization with tentative links to Whin Sill magmatism.

The role of the Burtreeford Disturbance

Recent analysis of the metamorphism associated with the Whin Sill (Robinson 2020) has questioned the traditional view that the Whin Sill magma ascended along feeder dykes located at the edge of the Alston Block. These studies have shown that contact metamorphism, forming an assemblage of grossular garnet, epidote, clinopyroxene, hedenbergite, prehnite and datolite, is thickest (up to 20 m) towards the centre of the Alston Block, suggesting that an ascending Whin Sill magma and associated high-temperature fluids were focused in this area close to the Burtreeford Disturbance.

Table 2: *Synopsis of the Sm and Nd fluorite data from the Slitt, Groverake and Ferney Gill veins, Whin Sill and limestone presented by Halliday et al. (1990)*

Sample	$^{147}Sm/^{144}Nd$	±2σ (abs)*	$^{143}Nd/^{144}Nd$	±2σ (abs)	$^{143}Nd/^{144}Nd_i$ at 291.5 Ma	±	εNd at 291.5 Ma
Slitt Vein							
B5	0.2172	0.0022	0.51221	0.00002	0.51180	0.00002	−9.1
B13	0.2232	0.0022	0.51218	0.00002	0.51175	0.00002	−9.9
B44	0.2513	0.0025	0.51223	0.00002	0.51175	0.00002	−10.0
B53	0.2841	0.0028	0.51228	0.00002	0.51174	0.00002	−10.2
B75	0.1875	0.0019	0.51220	0.00002	0.51184	0.00002	−8.2
B11	0.3214	0.0032	0.51232	0.00002	0.51171	0.00002	−10.9
B48	0.2147	0.0021	0.51218	0.00002	0.51177	0.00002	−9.6
B74	0.1540	0.0015	0.51202	0.00002	0.51173	0.00002	−10.5
B3	0.2009	0.0020	0.51216	0.00002	0.51178	0.00002	−9.5
B46	0.2295	0.0023	0.51219	0.00002	0.51175	0.00002	−10.0
B50	0.2936	0.0029	0.51223	0.00002	0.51167	0.00002	−11.6
Groverake Vein							
929	0.4027	0.0040	0.51229	0.00002	0.51152	0.00002	−14.5
480	0.2611	0.0026	0.51226	0.00002	0.51176	0.00002	−9.8
853	0.2738	0.0027	0.51227	0.00003	0.51175	0.00003	−10.1
858	0.2972	0.0030	0.51228	0.00003	0.51171	0.00003	−10.7
Ferney Gill Vein							
933*	0.3763	0.0038	0.51229	0.00001	0.51157	0.00001	−13.5
943*	0.2125	0.0021	0.51215	0.00001	0.51174	0.00001	−10.1
949*	0.3494	0.0035	0.51224	0.00001	0.51157	0.00001	−13.5
951*	0.4712	0.0047	0.51226	0.00001	0.51136	0.00001	−17.6
1050	0.4357	0.0044	0.51221	0.00003	0.51138	0.00003	−17.3
Whin Sill							
Dolerite	0.1326	0.0013	0.51249	0.00002	0.51224	0.00002	−0.5
Dolerite	0.1418	0.0014	0.5126	0.00002	0.51233	0.00002	1.3
Limestone							
Limestone	0.1653	0.0017	0.51207	0.00003	0.51175	0.00003	−9.9

*It should be noted that Halliday *et al.* (1990) did not report uncertainty. We estimate 1% absolute (2σ level) uncertainty.

The Whin Sill is also emplaced as a small laccolithic mass at Cowshill, where the Breckonsike Vein occupies the Burtreeford structure for a surface strike length of *c.* 2 km adjacent to which extensive metasomatic replacements of the Great Limestone by siderite and/or ankerite occur. Two other major mineralized structures diverge from the eastern side of the Burtreeford Disturbance at Cowshill. The NE–SW-trending Burtree Pasture Vein was extensively mined here for both lead and fluorspar. About 4 km to the NE this vein unites with the triple junction of the Red, Greencleugh and Groverake veins of the Red Vein Quarter Point set at Groverake in the Rookhope Valley (Fig. 1c). Although not known to carry significant mineralization in the near-surface strata in the interval between Cowshill and Groverake, this vein could conceivably have channelled mineralizing fluids at depth from the Burtreeford Disturbance towards the Groverake junction, which Dunham (1990) suggested to be a major emanative centre of mineralization, a model for which fluid inclusion and REE data give strong support (Smith 1974; Greenwood and Smith 1977). It is also significant that the roughly ESE–WNW Sedling Vein, at the western extremity of the Slitt Vein Quarter Point system, also originates from the eastern side of the Burtreeford Disturbance at Cowshill. The possibility that this too could have acted as a significant channel for mineralizing fluids from the Burtreeford structure is consistent with speculation on the role of Quarter Point veins as important feeders for mineralization.

At Allenheads, *c.* 4 km north of Cowshill, a complex of rich lead-bearing veins and associated 'flat' deposits in the Great Limestone connect with the eastern side of the Burtreeford Disturbance. All were worked at Allenheads Mine, the largest and most productive of the orefield's lead mines. Although Dunham (1990, p 167) recorded an underground driveage through the disturbance, no mineralization was encountered and the limited contemporary evidence was interpreted as indicating that the Allenheads veins terminated against the disturbance. The apparent absence of mineralization within the disturbance here may be due to the driveage being within beds above the Great Limestone that are typically unfavourable to mineralization. It is possible that the Allenheads deposits, together with those associated with their eastward continuation as the Red Vein Quarter Point system of the Rookhope Valley may, at least in part, have been fed via the Burtreeford Disturbance.

Thus there are a number of lines of evidence to suggest that the Burtreeford Disturbance, or a deep-rooted basement fault at depth that underlies it, acted as a significant conduit for both ascending magma associated with the Whin Sill complex and mineralizing fluids (Fig. 13b). The latter were then channelled away from the monocline into strike-slip related dilatational jogs and associated tensile veins of the ENE–WSW Lead Vein set and in particular the ESE–WNW Quarter Point vein set within the Alston Block.

Mineralization in the Cross Vein sets

Mineralization associated with Phase 1 NNW–SSE-trending 'Cross Veins' is generally sparse compared with that within Phase 2 fractures but there are two significant exceptions. First, the Leehouse Well–Sir John's Vein system of the South Tyne Valley exhibits significant mineralization at several points along its *c.* 10 km strike length. The galena is characterized by substantially higher silver concentrations than are normal for the NPO and the variety of copper sulfides, together with small amounts of bismuth, cobalt, nickel minerals and native silver have been interpreted as evidence of an early high-temperature phase of mineralization (Ixer *et al.* 1996; Fairbairn *et al.* 2020).

The second exception is the Nenthead area, where abundant lead–zinc–iron mineralization is present (see above). Although the higher temperature assemblages and more exotic metal content of the Leehouse Well–Sir John's vein assemblages have not been reported from Nenthead, this may be due to the current level of exposure. The deposits seen in the South Tyne Valley occur in much lower horizons within the Carboniferous succession than those of Nenthead, where it is conceivable that similar assemblages may be present at depth; traces of both nickel and cobalt supergene minerals have been reported here (Bridges and Young 1985).

Conclusions

New field and microstructural observations presented here suggest that the faults, fractures and mineralization of the Alston Block of the NPO record two distinct phases of deformation. During Phase 1, which is suggested to have occurred during the Late Carboniferous as a result of the far-field effects of the Variscan Orogeny, north–south shortening and basin inversion occurred, leading to folding and thrusting along the margins of the Alston Block (Fig. 13a). Phase 2 deformation was regionally coeval with Whin Sill magmatism at *c*. 297 Ma and the main phases of mineralization of the NPO in the Alston Block. This broad contemporaneity has been demonstrated by Re–Os analyses, which suggest that mineralization occurred at *c.* 294 Ma, and supported by recalculation of existing Sm–Nd fluorite data. This Early Permian event involved north–south lithospheric extension and east–west compression (Fig. 13b) and appears to be related to regional dextral transtensional reactivation of deep-seated NE–SW Caledonian basement structures as recognized in the adjacent Northumberland Basin (De Paola *et al.* 2005*a*). The North Pennine Orefield appears to be centred on the Burtreeford Disturbance, which may correspond to a deep-seated Caledonian structure in the basement that acted as a conduit for ascending metalliferous fluids in the earliest Permian.

The Re–Os isotopic analysis of the sulfide mineralization indicates that it is probably genetically linked to the primitive mantle source that gave rise to the Whin Sill magmatism. Previous interpretations of the NPO of the Alston Block as an MVT, or being caused by the influx of Zechstein seawater, although understandable given the obvious interactions with sedimentary host rocks during emplacement, are now thought to be incorrect. Based on the findings presented here, it is suggested that the NPO of the Alston Block should be regarded as having formed as a mantle magmatism associated F-rich deposit. The new genetic model proposed here suggests that the Alston Block is distinct from its southern neighbour, the Askrigg Block, where mineralization is less diverse, is associated with lower temperatures and seems to lack any clear link to mantle-derived fluids (e.g. Bau *et al.* 2003; Kraemer *et al.* 2019). This implies that the Alston and Askrigg blocks are genetically distinct and should be treated as two separate orefields.

It is significant that fluorine-associated orefields have been presumed to result from MVT mineralization in several other deposits across Europe and North Africa (e.g. Munoz *et al.* 1994, 1999; Subías and Fernández-Nieto 1995; Subías *et al.* 1998; Boiron *et al.* 2010; Souissi *et al.* 2010; Dill *et al.* 2011; Kraemer *et al.* 2019). It is now apparent that an important part of one of the supposedly archetypal examples is most probably related to mantle-sourced magmatism and fluorine-rich hydrothermal fluids and is therefore not a classic MVT. Reappraisal of other similar orefields worldwide may now be required.

Acknowledgements Thanks go to I. Chaplin for the preparation of thin sections for this project. Many thanks to reviewers Nigel Woodcock and Anonymous for their very helpful and constructive comments.

Author contributions **EDD**: data curation (lead), formal analysis (equal), investigation (lead), writing – original draft (equal); **REH**: conceptualization (lead), funding acquisition (lead), investigation (supporting), methodology (supporting), writing – original draft (equal), writing – review & editing (lead); **DS**: formal analysis (equal), investigation (supporting), methodology

(lead), writing – review & editing (supporting); **AB**: formal analysis (supporting), investigation (supporting); **BY**: conceptualization (supporting), investigation (supporting), writing – review & editing (supporting); **CLC**: investigation (supporting), methodology (supporting)

Funding This research received no specific grant from any funding agency in the public, commercial, or not-for-profit sectors.

Data availability All data generated or analysed during this study are included in this published article.

Scientific editing by John MacDonald

References

Adams, S.F. 1920. A microscopic study of vein quartz. *Economic Geology*, **15**, 623–664, https://doi.org/10.2113/gsecongeo.15.8.623

Alaniz-Alvarez, S.A., Nieto-Samaniego, Á.F. and Tolson, G. 1998. A graphical technique to predict slip along a pre-existing plane of weakness. *Engineering Geology*, **49**, 53–60, https://doi.org/10.1016/S0013-7952(97)00071-9

Angelier, J. 1979. Determination of the mean principal directions of stress for a given fault population. *Tectonophysics*, **156**, T17–T26, https://doi.org/10.1016/0040-1951(79)90081-7

Angelier, J. 1984. Tectonic analysis of fault slip data sets. *Journal of Geophysical Research: Solid Earth*, **89**, 5835–5848, https://doi.org/10.1029/JB089iB07p05835

Astle, J.M. 1978. *A Magnetic and Electromagnetic Survey of the Burtreeford Disturbance, Upper Teesdale*. MSc thesis, University of Durham.

Bau, M., Romer, R.L., Lüders, V. and Dulski, P. 2003. Tracing element sources of hydrothermal mineral deposits: REE and Y distribution and Sr–Nd–Pb isotopes in fluorite from MVT deposits in the Pennine Orefield, England. *Mineralium Deposita*, **38**, 992–1008, https://doi.org/10.1007/s00126-003-0376-x

Bevins, R.E., Young, B., Mason, J.S., Manning, D.A.C. and Symes, R.F. 2010. *Mineralization of England and Wales. Geological Conservation Review Series, No 36: The Mineralogy of Great Britain*. Joint Nature Conservation Committee, Peterborough.

Boiron, M.C., Cathelineau, M. and Richard, A. 2010. Fluid flows and metal deposition near basement/cover unconformity: lessons and analogies from Pb–Zn–F–Ba systems for the understanding of Proterozoic U deposits. *Geofluids*, **10**, 270–292, https://doi.org/10.1111/j.1468-8123.2010.00289.x

Bott, M.H. and Smith, F.W. 2018. The role of the Devonian Weardale Granite in the emplacement of the North Pennine mineralization. *Proceedings of the Yorkshire Geological Society*, **62**, 1–15, https://doi.org/10.1144/pygs2017-391

Bott, M.P., Swinburn, P.M. and Long, R.E. 1984. Deep structure and origin of the Northumberland and Stainmore troughs. *Proceedings of the Yorkshire Geological Society*, **44**, 479–495, https://doi.org/10.1144/pygs.44.4.479

Bouch, J.E., Naden, J., Shepherd, T.J., McKervey, J.A., Young, B., Benham, A.J. and Sloane, H.J. 2006. Direct evidence of fluid mixing in the formation of stratabound Pb–Zn–Ba–F mineralisation in the Alston Block, North Pennine Orefield (England). *Mineralium Deposita*, **41**, 821–835, https://doi.org/10.1007/s00126-006-0093-3

Boyle, R.W. 1979. *The geochemistry of gold and its deposits*. Canada Geological Survey Bulletin, **280**.

Bridges, T.F. and Young, B. 1985. Supergene minerals of the Northern Pennine Orefield – A review. *Journal of the Russell Society*, **7**, 3–14.

Cann, J.R. and Banks, D.A. 2001. Constraints on the genesis of the mineralization of the Alston Block, Northern Pennine Orefield, northern England. *Proceedings of the Yorkshire Geological Society*, **53**, 187–196, https://doi.org/10.1144/pygs.53.3.187

Chadwick, R.A., Holliday, D.W., Holloway, S. and Hulbert, A.G. 1995. *The structure and evolution of the Northumberland–Solway Basin and adjacent areas. Subsurface Memoir of the British Geological Survey*. British Geological Survey, Keyworth.

Collier, R.L. 1989. Tectonic evolution of the Northumberland Basin; the effects of renewed extension upon an inverted extensional basin. *Journal of the Geological Society, London*, **146**, 981–989, https://doi.org/10.1144/gsjgs.146.6.0981

Corfield, S.M., Gawthorpe, R.L., Gage, M., Fraser, A.J. and Besly, B.M. 1996. Inversion tectonics of the Variscan foreland of the British Isles. *Journal of the Geological Society, London*, **153**, 17–32, https://doi.org/10.1144/gsjgs.153.1.0017

Cornwell, J.D. and Wadge, A.J. 1980. *Geophysical Investigations in the Closehouse–Lunedale Area*. Report **WF/MR/80/031**. Institute of Geological Sciences, London.

Critchley, M.F. 1984. Variscan tectonics of the Alston Block, northern England. *Geological Society, London, Special Publications*, **14**, 139–146, https://doi.org/10.1144/GSL.SP.1984.014.01.14

Crowley, S.F., Bottrell, S.H., McCarthy, B., Ward, J. and Young, B. 1997. $\delta^{34}S$ of Lower Carboniferous anhydrite, Cumbria and its implications for barite mineralization in the northern Pennines. *Journal of the Geological Society, London*, **154**, 597–600, https://doi.org/10.1144/gsjgs.154.4.0597

Davison, J.M., Ineson, P.R. and Mitchell, J.G. 1992. Potassium–argon isotopic age determinations from the metasomatic alteration of the Great Limestone, Northern Pennine Orefield. *Proceedings of the Yorkshire Geological Society*, **49**, 71–74, https://doi.org/10.1144/pygs.49.1.71

Dempsey, E.D., Holdsworth, R.E., Imber, J., Bistacchi, A. and Di Toro, G. 2014. A geological explanation for intraplate earthquake clustering complexity: The zeolite-bearing fault/fracture networks in the Adamello Massif (Southern Italian Alps). *Journal of Structural Geology*, **66**, 58–74, https://doi.org/10.1016/j.jsg.2014.04.009

De Paola, N., Holdsworth, R.E., McCaffrey, K.J. and Barchi, M.R. 2005*a*. Partitioned transtension: an alternative to basin inversion models. *Journal of Structural Geology*, **27**, 607–625, https://doi.org/10.1016/j.jsg.2005.01.006

De Paola, N., Holdsworth, R.E. and McCaffrey, K.J.W. 2005*b*. The influence of lithology and pre-existing structures on reservoir-scale faulting patterns in transtensional rift zones. *Journal of the Geological Society, London*, **162**, 471–480, https://doi.org/10.1144/0016-764904-043

Dichiarante, A.M., Holdsworth, R.E. *et al.* 2016. New structural and Re–Os geochronological evidence constraining the age of faulting and associated mineralization in the Devonian Orcadian Basin, Scotland. *Journal of the Geological Society, London*, **173**, 457–473, https://doi.org/10.1144/jgs2015-118

Dichiarante, A.M., Holdsworth, R.E., Dempsey, E., McCaffrey, K.J.W. and Utley, T.A.G. 2020. Outcrop-scale manifestations of reactivation during multiple superimposed rifting and basin inversion events: the Devonian Orcadian Basin, N Scotland. *Journal of the Geological Society, London*, **178**, https://doi.org/10.1144/jgs2020-089

Dill, H.G., Hansen, B.T. and Weber, B. 2011. REE contents, REE minerals and Sm/Nd isotopes of granite- and unconformity-related fluorite mineralization at the western edge of the Bohemian Massif: with special reference to the Nabburg–Wölsendorf district, SE Germany. *Ore Geology Reviews*, **40**, 132–148, https://doi.org/10.1016/j.oregeorev.2011.06.003

Dunham, K.C. 1931. Mineral deposits of the North Pennine. *Proceedings of the Geologists' Association*, **42**, 274.

Dunham, K.C. 1934. The genesis of the north Pennine ore deposits. *Quarterly Journal of the Geological Society of London*, **90**, 689–720, https://doi.org/10.1144/GSL.JGS.1934.090.01-04.23

Dunham, K.C. 1944. The production of galena and associated minerals in the Northern Pennines; with comparative statistics for Great Britain. *Transactions of the Institution of Mining and Metallurgy*, **51**, 181–252.

Dunham, K.C. 1983. Ore genesis in the English Pennines: a fluoritic subtype. Proceedings of the International Conference on Mississippi Valley Type Lead–Zinc deposits, Rolla, Missouri, 86–112.

Dunham, K.C. 1990. *Geology of the Northern Pennine Orefield: Volume 1 Tyne to Stainmore*. Economic Memoir of the British Geological Survey, England and Wales, Sheets 19 and 25, and parts of 13, 24, 26, 31, 32. 2nd edition.

Dunham, K.C., Johnson, G.A.L., Bott, M.H.P. and Hodge, B.L. 1961. Granite beneath the northern Pennine. *Nature*, **190**, 899–900, https://doi.org/10.1038/190899a0

Dunham, K.C., Dunham, A.C., Hodge, B.L. and Johnson, G.A.L. 1965. Granite beneath Viséan sediments with mineralization at Rookhope, northern Pennine. *Quarterly Journal of the Geological Society*, **121**, 383–414, https://doi.org/10.1144/gsjgs.121.1.0383

Dunham, K.C., Fitch, F.J., Miller, J.A. and Mitchell, J.G. 1968. The geochronological significance of argon-40/argon-39 age determinations on white whin from the northern-Pennine orefield. *Proceedings of the Royal Society of London*, **307**, 251–266.

Fairbairn, R.A., Ixer, R.A. and Young, B. 2020. Ore mineralogy of the Clargillhead Vein, Tynehead, Cumbria: the first report of native silver from the Northern Pennine Orefield. *Journal of the Russell Society*, **23**, 48–52.

Francis, E.H. 1982. Magma and sediment – I. Emplacement mechanism of late Carboniferous tholeiite sills in northern Britain: President's anniversary address 1981. *Journal of the Geological Society, London*, **139**, 1–20, https://doi.org/10.1144/gsjgs.139.1.0001

Frenzel, M. and Woodcock, N.H. 2014. Cockade breccia: product of mineralisation along dilational faults. *Journal of Structural Geology*, **68**, 194–206, https://doi.org/10.1016/j.jsg.2014.09.001

Greenwood, D. and Smith, F.W. 1977. Fluorspar mining in the northern Pennines. *Transactions of the Institution of Mining and Metallurgy*, **86**, B181–B190.

Gupta, M.C. and MacFarlane, R.D. 1970. The natural alpha radioactivity of samarium. *Journal of Inorganic and Nuclear Chemistry*, **32** , 3425–3432, https://doi.org/10.1016/0022-1902(70)80149-X

Halliday, A., Shepherd, T., Dickin, A. *et al.*. 1990. Sm–Nd evidence for the age and origin of a Mississippi Valley Type ore deposit. *Nature,* **344**, 54–56, https://doi.org/10.1038/344054a0

Hamilton, M.A. and Pearson, D.G. 2011. Precise U–Pb age for the Great Whin Dolerite Complex, NE England and its significance. *In*: Srivastava, R.K. (ed.) *Dyke Swarms: Keys for Geodynamic Interpretation*. Springer, Berlin, 495–507.

Hill, J.A. and Dunham, K.C. 1968. The barites deposits at Closehouse, Lunedale, Yorkshire. *Proceedings of the Yorkshire Geological Society*, **36**, 351–372, https://doi.org/10.1144/pygs.36.3.351

Hnatyshin, D., Creaser, R.A., Wilkinson, J.J. and Gleeson, S.A. 2015. Re–Os dating of pyrite confirms an early diagenetic onset and extended duration of

mineralization in the Irish Zn–Pb ore field. *Geology*, **43**, 143–146, https://doi.org/10.1130/G36296.1

Holdsworth, R.E., Dempsey, E. *et al.* 2015. Silurian–Devonian magmatism, mineralization, regional exhumation and brittle strike-slip deformation along the Loch Shin Line, NW Scotland. *Journal of the Geological Society, London*, **172**, 748–762, https://doi.org/10.1144/jgs2015-058

Holdsworth, R.E., Selby, D., Dempsey, E., Scott, L., Hardman, K., Fallick, A.E. and Bullock, R. 2020. The nature and age of Mesoproterozoic strike-slip faulting based on Re–Os geochronology of syntectonic copper mineralization, Assynt Terrane, NW Scotland. *Journal of the Geological Society, London*, **177**, 686–699, https://doi.org/10.1144/jgs2020-011

Ixer, R.A., Young, B. and Stanley, C.J. 1996. Bismuth-bearing assemblages from the Northern Pennine Orefield. *Mineralogical Magazine*, **60**, 317–324, https://doi.org/10.1180/minmag.1996.060.399.06

Johnson, G.A.L. and Dunham, K.C. 1963. The geology of Moor House. *Nature Conservancy Monograph No 2*. London HMSO.

Johnson, G.A.L. and Dunham, K.C. 2001. Emplacement of the Great Whin Dolerite Complex and the Little Whin Sill in relation to the structure of northern England. *Proceedings of the Yorkshire Geological Society*, **53**, 177–186, https://doi.org/10.1144/pygs.53.3.177

Kimbell, G.S., Young, B., Millward, D. and Crowley, Q.G. 2010. The North Pennine batholith (Weardale Granite) of northern England: new data on its age and form. *Proceedings of the Yorkshire Geological Society*, **58**, 107–128, https://doi.org/10.1144/pygs.58.1.273

Kraemer, D., Viehmann, S., Banks, D., Sumoondur, A.D., Koeberl, C. and Bau, M. 2019. Regional variations in fluid formation and metal sources in MVT mineralization in the Pennine Orefield, UK: Implications from rare earth element and yttrium distribution, Sr–Nd isotopes and fluid inclusion compositions of hydrothermal vein fluorites. *Ore Geology Reviews*, **107**, 960–972, https://doi.org/10.1016/j.oregeorev.2019.03.014

Ludwig, K. R. 1980. Calculation of uncertainties of U–Pb isotope data. *Earth and Planetary Science Letters*, **46**, 212–220, https://doi.org/10.1016/0012-821X(80)90007-2

Meisel, T., Walker, R.J. and Morgan, J.W. 1996. The osmium isotopic composition of the Earth's primitive upper mantle. *Nature*, **383**, 517–520, https://doi.org/10.1038/383517a0

Michael, A.J. 1984. Determination of stress from slip data: faults and folds. *Journal of Geophysical Research: Solid Earth*, **89**, 11517–11526, https://doi.org/10.1029/JB089iB13p11517

Morgan, P.G. 1925. The so-called 'pseudomorphous' quartz of Tertiary gold–silver veins. *Economic Geology*, **20**, 203–207, https://doi.org/10.2113/gsecongeo.20.3.203

Moseley, F. 1972. A tectonic history of northwest England. *Journal of the Geological Society, London*, **128**, 561–594, https://doi.org/10.1144/gsjgs.128.6.0561

Munoz, M., Boyce, A.J., Courjault-Radé, P., Fallick, A.E. and Tollon, F. 1994. Multi-stage fluid incursion in the Palaeozoic basement-hosted Saint-Salvy ore deposit (NW Montagne Noire, southern France). *Applied Geochemistry*, **9**, 609–626, https://doi.org/10.1016/0883-2927(94)90022-1

Munoz, M., Boyce, A.J., Courjault-Radé, P., Fallick, A.E. and Tollon, F. 1999. Continental basinal origin of ore fluids from southwestern Massif central fluorite veins (Albigeois, France): evidence from fluid inclusion and stable isotope analyses. *Applied Geochemistry*, **14**, 447–458.

Robinson, D. 2020. Whin Sill Contact Metamorphism in the Cow Green Reservoir boreholes, Northern England – evidence for an Upper Teesdale source for the Whin Sill magma. *Proceedings of the Yorkshire Geological Society*, **63**, pygs2019-018, https://doi.org/10.1144/pygs2019-018

Rogers, A.F. 1917. A review of the amorphous minerals. *Journal of Geology*, **15**, 515–541, https://doi.org/10.1086/622518

Selby, D., Conliffe, J., Crowley, Q.G. and Feely, M. 2008. Geochronology (Re–Os and U–Pb) and fluid inclusion studies of molybdenite mineralisation associated with the Shap, Skiddaw and Weardale granites, UK. *Applied Earth Science*, **117**, 11–28, https://doi.org/10.1179/174327508X309669

Selby, D., Kelley, K.D., Hitzman, M.W. and Zieg, J. 2009. Re–Os sulfide (bornite, chalcopyrite, and pyrite) systematics of the carbonate-hosted copper deposits at Ruby Creek, southern Brooks Range, Alaska. *Economic Geology*, **104**, 437–444, https://doi.org/10.2113/gsecongeo.104.3.437

Shepherd, T.J., Darbyshire, D.P.F., Moore, G.R. and Greenwood, D.A. 1982. Rare earth element and isotopic geochemistry of the North Pennine ore deposits. *Bulletin du Bureau des Recherches Géologiques et Minières*, **2**, 371–377.

Shiells, K.A.G. 1963. The Geological Structure of North-East Northumberland. *Earth and Environmental Science Transactions of the Royal Society of Edinburgh*, **65**, 449–481, https://doi.org/10.1017/S0080456800012709

Smirnov, V.I. 1954. *Geologicheskie osnovy polskov i razvedok rudnykh mestorozhdenĭ*. Izdvo Moskovskogo Universiteta.

Smith, F.W. 1974. Yttrium content of fluorite as a guide to vein intersections in partially developed fluorspar ore bodies. *Transactions of the Society of Mining Engineers*, **255**, 95–96.

Smoliar, M.I., Walker, R.J. and Morgan, J.W. 1996. Re–Os ages of group IIA, IIIA, IVA, and IVB iron meteorites. *Science*, **271**, 1099–1102, https://doi.org/10.1126/science.271.5252.1099

Solomon, M., Rafter, T. A. and Dunham, K. C. 1971. Sulphur and oxygen isotope studies in the northern Pennine in relation to ore genesis. *Transactions of the Institution of Mining and Metallurgy*, **80**, B258–B275.

Souissi, F., Souissi, R. and Dandurand, J.-L. 2010. The Mississippi Valley-type fluorite ore at Jebel Stah (Zaghouan district, north-eastern Tunisia): contribution of REE and Sr isotope geochemistries to the genetic model. *Ore Geology Reviews*, **37**, 15–30, https://doi.org/10.1016/j.oregeorev.2009.11.001

Subías, I. and Fernández-Nieto, C. 1995. Hydrothermal events in the Valle de Tena (Spanish Western Pyrenees) as evidenced by fluid inclusions and trace-element distribution from fluorite deposits. *Chemical Geology*, **124**, 267–282, https://doi.org/10.1016/0009-2541(95)00060-Y

Subías, I., Moritz, R. and Fernández-Nieto, C. 1998. Isotopic composition of strontium in the Valle de Tena (Spanish Central Pyrenees) fluorite deposits: relevance for the source of elements and genetic significance. *Mineralium Deposita*, **33**, 416–424, https://doi.org/10.1007/s001260050159

Thomas, C.W. and Woodcock, N.H. 2015. *Proceedings of the Yorkshire Geological Society*, **60**, 258–274, https://doi.org/10.1144/pygs2015-358

Thorpe, R.S. and MacDonald, R. 1985. Geochemical evidence for the emplacement of the Whin Sill complex of northern England. *Geological Magazine*, **122**, 389–396, https://doi.org/10.1017/S0016756800031836

Timmerman, M.J. 2004. Timing, geodynamic setting and character of Permo-Carboniferous magmatism in the foreland of the Variscan Orogen, NW Europe. *Geological Society, London, Special Publications*, **223**, 41–74, https://doi.org/10.1144/GSL.SP.2004.223.01.03

Underhill, J.R., Gayer, R.A., Woodcock, N.H., Donnelly, R., Jolley, E. and Stimpson, I.G. 1988. The Dent Fault, northern England—reinterpreted as a major oblique slip fault zone. *Journal of the Geological Society, London*, **145**, 313–316.

Vermeesch, P. 2018. IsoplotR: A free and open toolbox for geochronology. *Geoscience Frontiers*, **9**, 1479–1493, https://doi.org/10.1016/j.gsf.2018.04.001

Warr, L. 2012. The Variscan Orogeny: the welding of Pangaea. *In*: Woodcock, N.H. and Strachan, R.A. (eds) *Geological History of Britain and Ireland*. Wiley–Blackwell, Chichester, 274–298.

Woodcock, N.H. and Rickards, B. 2003. Transpressive duplex and flower structure: Dent Fault System, NW England. *Journal of Structural Geology*, **25**, 1981–1992, https://doi.org/10.1016/S0191-8141(03)00057-9

Woodcock, N. H., Miller, A. V. and Woodhouse, C.D. 2014. Chaotic breccia zones on the Pembroke Peninsula, South Wales: collapse into voids along dilational faults. *Journal of Structural Geology*, **69**, 91–107, https://doi.org/10.1016/j.jsg.2014.09.019

Young, B. 2017. Magnetite mineralisation associated with The Great Whin Sill of Upper Teesdale, Northern Pennines. *Journal of the Russell Society*, **20**, 57–64.

Young, B. and Hopkirk, A. 2019. Epimorphs and pseudomorphs after fluorite from the Northern Pennine Orefield. *Journal of the Russell Society*, **22**, 96–104.

Young, B., Styles, M.T. and Berridge, N.G. 1985. Niccolite–magnetite mineralization from Upper Teesdale, North Pennines. *Mineralogical Magazine*, **49**, 555–559, https://doi.org/10.1180/minmag.1985.049.353.09